



An experimental and kinetic modeling study of combustion of isomers of butanol

Roberto Grana^a, Alessio Frassoldati^a, Tiziano Faravelli^a, Ulrich Niemann^b, Eliseo Ranzi^{a,*}, Reinhard Seiser^b, Robert Cattolica^b, Kalyanasundaram Seshadri^b

^a Dipartimento di Chimica, Materiali e Ingegneria Chimica, Politecnico di Milano, Milano, Italy

^b Department of Mechanical and Aerospace Engineering, University of California at San Diego, La Jolla, CA 92093-0411, USA

ARTICLE INFO

Article history:

Received 16 February 2010

Received in revised form 22 April 2010

Accepted 17 May 2010

Available online 10 June 2010

Keywords:

Butanol isomers
Kinetic modeling
Flame structure
Bio-fuels

ABSTRACT

A kinetic model is developed to describe combustion of isomers of butanol—n-butanol (n-C₄H₉OH), sec-butanol (sec-C₄H₉OH), iso-butanol (iso-C₄H₉OH), and tert-butanol (tert-C₄H₉OH). A hierarchical approach is employed here. This approach was previously found to be useful for developing detailed and semi-detailed mechanism of oxidation of various hydrocarbon fuels. This method starts from lower molecular weight compounds of a family of species and proceeds to higher molecular weight compounds. The pyrolysis and oxidation mechanisms of butanol isomers are similar to those for hydrocarbon fuels. Here, the development of the complete set of the primary propagation reactions for butanol isomers proceeds from the extension of the kinetic parameters for similar reactions already studied and recently revised for ethanol, n-propanol and iso-propanol. A detailed description leading to evaluation of rate constants for initiation reactions, metathesis reactions, decomposition reactions of alkoxy radicals, isomerization reactions, and four-center molecular dehydration reactions are given. Decomposition and oxidation of primary intermediate products are described using a previously developed semi-detailed kinetic model for hydrocarbon fuels. The kinetic mechanism is made up of more than 7000 reactions among 300 species. The model is validated by comparing predictions made using this kinetic model with previous and new experimental data on counterflow non-premixed flames of n-butanol and iso-butanol. The structures of these flames were measured by removing gas samples from the flame and analyzing them using a gas chromatograph. Temperature profiles were measured using coated thermocouples. The flame structures were measured under similar conditions for both fuels to elucidate the similarities and differences in combustion characteristics of the two isomers. The profiles measured include those of butanol, oxygen, carbon dioxide, water vapor, carbon monoxide, hydrogen, formaldehyde, acetaldehyde, and a number of C₁–C₄ hydrocarbon compounds. The predictions of the kinetic model of flame structures of the two isomers were satisfactory. Validation of the kinetic model was also performed by comparing predictions with experimental data reported in the literature. These data were obtained in batch reactors, flow reactors, jet-stirred reactors, and shock tubes. In these configurations, combustion is not influenced by molecular transport. The agreement between the kinetic model and experimental data was satisfactory.

© 2010 The Combustion Institute. Published by Elsevier Inc. All rights reserved.

1. Introduction

Recent interest in promoting the use of bio-fuels arises from the need to improve energy security and reduce net greenhouse gas emissions. At the present rate of energy consumption, worldwide reserves of natural gas, oils and to a limited extent coal are rapidly diminishing. This process is being accelerated by significant increases in the rates of energy consumption in developing countries. These developments have increased the cost of fossil fuels and have an adverse impact on the national economies of the world. Thus, there is a need to decrease the use of fossil fuels for sustainable development, and allow future generations to continue the

use of fossil fuels. Recent legislation in many countries require them to limit emissions of greenhouse gases. Bio-fuels are carbon neutral, thus they are considered to be more environmentally friendly and help in meeting legislative requirements by limiting emissions of greenhouse gases. Both EU and USA are committed to reducing energy consumption and to increase renewable fuel use. All these point to increasing use of bio-fuels in the near future.

Alcohols show significant potential to be an alternative to conventional gasoline. Alcohols are renewable fuels because they can be produced from biomass fermentation and are by-products of Fischer Tropsch processes. Ethanol is currently a component of reformulated gasoline. The amount of ethanol in gasoline is projected to increase in the future. There is considerable interest in promoting the use of butanol (C₄H₉OH) as an alternative to ethanol. Butanol can be derived from lignocellulosic materials. Butanol

* Corresponding author.

E-mail address: eliseo.ranzi@polimi.it (E. Ranzi).

has some advantages, as transportation fuel component, when compared with ethanol. It is less corrosive, has a lower vapor pressure, higher energy density, and its octane rating is similar to that of gasoline. Thus, it can be blended with gasoline at much higher proportions than ethanol without compromising efficiency. Butanol is immiscible when mixed with water at concentrations higher than about 7–8%. This eliminates a number of storage concerns and makes phase separation considerably easier in comparison to ethanol. Unfortunately, butanol has a foul odor that can persist for a long time. Butanol is yet to be employed as extensively as ethanol as transportation fuel, because the production of butanol is labor intensive and only low yields have been achieved. These limitations are expected to improve in the near future.

Numerous studies have addressed combustion of methanol [1–6], ethanol [1,7–14] and propanol isomers [15]. These studies provide the building blocks for the kinetic modeling of combustion of butanol isomers. The isomers of butanol are n-butanol (n-C₄H₉OH), sec-butanol (sec-C₄H₉OH), iso-butanol (iso-C₄H₉OH), and tert-butanol (tert-C₄H₉OH). Dagaut and Togbé [16] developed a sub-mechanism for n-butanol, which was combined with an overall kinetic mechanism of oxidation of gasoline. Moss et al. [17] have proposed a detailed kinetic scheme for describing the high-temperature oxidation of the different butanol isomers. Recently, Black et al. [18] have tested predictions of a kinetic model of n-butanol oxidation with autoignition delay times measured in shock tubes, and data on evolution of various species measured in a jet-stirred reactor, with encouraging results. These studies [16–18] were restricted to premixed systems without flow. Studies on premixed combustion with molecular transport are available [19,20]. McEnally and Pfefferle [19] studied pollutant emissions from methane/air flames doped with the four butanol isomers. Yang et al. [20] studied laminar premixed, low-pressure flames of the four butanol isomers, by using photoionization mass spectrometry. The structures of non-premixed n-butanol flames in non-uniform flows were measured previously employing the counterflow configuration [21]. The structure of non-premixed flames depends on the stoichiometric mixture fraction, Z_{st} , and the strain rate [22–24]. The previous measurements of the structure of n-butanol flames were made with the oxidizer stream made up of air enriched with oxygen [21]. The experimental conditions were characterized by high values of the stoichiometric mixture fraction and low values of the strain rates. Combustion in practical systems are characterized by low values of the stoichiometric mixture fraction and both low and high values of the strain rates [25]. To complement the previous studies, new experimental data on the structures of counterflow non-premixed flames of n-butanol and iso-butanol are shown here. The flame structures are measured with air as the oxidizer. The experimental conditions are characterized by low values of stoichiometric mixture fraction, and moderately high values of strain rate. The new experimental data allows comparison of the flame structures of butanol isomers. The new experimental data together with previous experimental data are helpful for validating the kinetic model of alcohol fuels.

A hierarchical approach is found to be useful for developing detailed and semi-detailed mechanism for describing oxidation of various fuels. This method starts from lower molecular weight compounds of a family of species and proceeds to higher molecular weight compounds. This procedure allows extensions to other compounds using similarity and analogy rules. Using this procedure, validated kinetic mechanisms of oxidation of ethanol [14] and propanol isomers have been developed [15]. Here, an oxidation scheme that considers the primary reactions of the four butanol isomers is proposed and tested. This kinetic mechanism is analogue and aligned with those of the lower alcohols. This is a further step towards the confirmation of the proposed classes of

reactions and of their rate constants, with a particular attention to H abstraction and molecular dehydration reactions.

2. Experimental measurements of flame structure

The structures of non-premixed flames of n-butanol and iso-butanol were measured employing the counterflow configuration. Fig. 1 shows a schematic illustration of the counterflow configuration. Steady, axisymmetric, laminar flow of two counterflowing streams toward a stagnation plane is considered. In this configuration, a fuel stream made up of pre-vaporized fuel (n-butanol or iso-butanol) and nitrogen is injected from the fuel duct, and an oxidizer stream of air is injected from the oxidizer duct. These jets flow into the mixing layer between the two ducts. The exit of the fuel duct is called the fuel boundary and the exit of the oxidizer duct the oxidizer boundary. Fine wire meshes are placed at the exits of the ducts. As a consequence, the tangential component of the flow velocities vanishes at the boundaries. This allows the use of “plug flow boundary conditions” in the numerical simulations of the flame structure. The mass fraction of fuel, the temperature, and the component of the flow velocity normal to the stagnation plane at the fuel boundary are represented by $Y_{F,1}$, T_1 , and V_1 , respectively. The mass fraction of oxygen, the temperature, and the component of the flow velocity normal to the stagnation plane at the oxidizer boundary are represented by $Y_{O_2,2}$, T_2 , and V_2 , respectively. The exit diameter of the fuel duct and the oxidizer duct is 23.3 mm. The distance between the fuel boundary and the oxidizer boundary is represented by L .

The value of the strain rate, defined as the normal gradient of the normal component of the flow velocity, changes from the fuel boundary to the oxidizer boundary [26]. The characteristic strain rate on the oxidizer side of the stagnation plane a_2 is given by [26]

$$a_2 = (2|V_2|/L)[1 + |V_1|\sqrt{\rho_1}/(|V_2|\sqrt{\rho_2})]. \quad (1)$$

Here, ρ_1 and ρ_2 represent the density of the mixture at the fuel boundary and at the oxidizer boundary, respectively. The stoichiometric mixture fraction, Z_{st} is [22–24]

$$Z_{st} = (1 + \nu Y_{F,1}/Y_{O_2,2})^{-1}. \quad (2)$$

where ν is the stoichiometric mass ratio of oxygen to fuel. For stoichiometric combustion of butanol, $\nu = 2.5946$.

The profiles of concentration of stable species were measured for $Y_{F,1} = 0.3$, $T_1 = 353$ K, $Y_{O_2,2} = 0.233$, $T_2 = 298$ K, $a_2 = 100$ s⁻¹, $V_1 = 0.248$ m/s, $V_2 = 0.25$ m/s, and $L = 10$ mm. At these conditions, the flame is on the oxidizer side of the stagnation plane with the stoichiometric mixture fraction $Z_{st} = 0.23$. Fig. 2 shows the photograph of a n-butanol flame stabilized in the counterflow burner. Concentrations profiles of stable species were measured by remov-

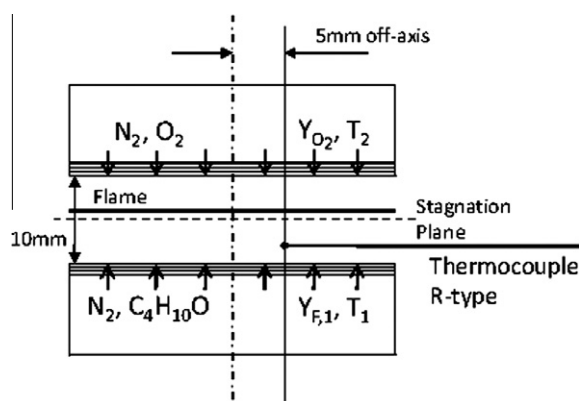


Fig. 1. Schematic illustration of the counterflow configuration. The figure shows the thermocouple, used for measuring flame temperature.

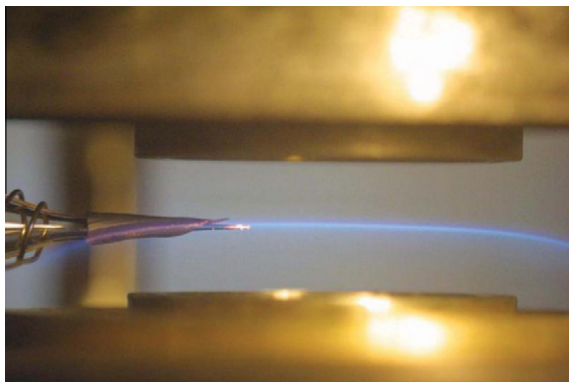


Fig. 2. Photograph of a non-premixed n-butanol flame stabilized in the counterflow burner for $Y_{F,1} = 0.3$, $T_1 = 353$ K, $Y_{O_2,2} = 0.233$, $T_2 = 298$ K, $a_2 = 100$ s⁻¹, $V_1 = 0.248$ m/s, $V_2 = 0.25$ m/s, and $L = 10$ mm. The figure shows the quartz microprobe.

ing gas samples from the reaction zone using a heated quartz microprobe, and analyzing them in a gas chromatograph. All lines from the sample probe to the gas chromatograph were heated to 373 K. The microprobe has a tip with an inner diameter of 150 μ m. To minimize disturbances to the flow-field, the tip of the microprobe was placed at a location of 5 mm off the axis of symmetry as shown in Figs. 1 and 2. The location of the sampling probe in the flow-field was determined using a digital photo camera.

The size of one pixel in the camera corresponds to a distance of approximately 20 μ m in the flow-field. The mole fractions of various species in the sample were measured using an Agilent 3000-microGC gas chromatograph. This instrument is equipped with a 10 m long molecular sieve 5A column, a 8 m long Poraplot U column, a 8 m long Poraplot Q column, and a 8 m long OV-1 column. The gas chromatograph has a built-in sample pump. To ensure equal sample sizes and thus comparable results across all measurements, a constant sample inlet pressure is required. Therefore, species were sampled at a constant pressure of 600 mbar into a sample vessel. Nitrogen was then introduced until the vessel attained a total pressure of 1150 mbar. After a waiting period of 6 min, to allow sufficient mixing, the sample was introduced into the gas chromatograph. The molecular sieve column uses argon as a carrier gas. It was used to separate hydrogen (H₂), oxygen (O₂), nitrogen (N₂), methane (CH₄), and carbon monoxide (CO). All other columns use helium as a carrier gas. The Poraplot U column was used for separating carbon dioxide (CO₂), ethene (C₂H₄), ethane (C₂H₆), ethyne (C₂H₂), and formaldehyde (CH₂O). The Poraplot Q column was used for separating water (H₂O), 1,2-propadiene (C₃H₄), propyne (C₃H₄), propene (C₃H₆), propane (C₃H₈), acetaldehyde (C₂H₄O), butene (C₄H₈), and butadiene (C₄H₆). The OV-1 column was used for separating butanal (n-C₃H₇CHO), n-butanol and iso-butanol. The mole fractions of various species eluting from the columns were measured using thermal-conductivity detectors (TCD). The detectors were calibrated using samples of known composition. For those species that are gases at 298 K and pressure of 1 bar, the calibration was performed with calibration gases of known composition. For those species that are liquids at 298 K and 1 bar calibration was performed using a sample vessel. First, the sample vessel was evacuated. Next, the liquid was injected into the vessel with a syringe through a septum placed in the wall of the vessel. It was then diluted with nitrogen. The concentration of the species was established from the pressure of the vessel recorded after evaporation and the total pressure after nitrogen dilution. This procedure was used for n-butanol, iso-butanol, water, and formaldehyde. The peaks for all species presented here show very good separation. Therefore the expected accuracy for the maximum concentrations of all species except H₂O and

CH₂O is expected to be better than $\pm 10\%$. The expected accuracy for H₂O and CH₂O is $\pm 20\%$. The accuracy for formaldehyde is based on the signal size compared to the baseline noise. The calibration for formaldehyde showed very little deviation and good repeatability.

Temperature profiles were measured for n-butanol and iso-butanol flames, using a Platinum–Platinum13%Rhodium thermocouple (R-type), at conditions identical to those employed in the measurement of concentration profiles. As shown in Fig. 1, the measurements were made along a line that is parallel to the axis of symmetry and approximately 5 mm away from the axis. The exact location of the thermocouple bead was determined using a digital photo camera. The measurements were made with bare thermocouple wires (uncoated) as well as with coated thermocouple wires. The wire diameter of the bare (uncoated) thermocouple was 25 μ m and the bead diameter was 90 μ m. The coated thermocouple had a layer of BeO/Y₂O₃ to avoid catalytic reactions at the surface of the thermocouple [27]. The coating was performed following the procedure recommended in Ref. [27]. The wire diameter of the coated thermocouple was 35 μ m and the bead diameter was 135 μ m. The measured temperatures with both thermocouples were corrected by taking into consideration radiative heat losses from the surface of the thermocouple. The corrections were made employing the procedure described by Peterson and Laurendeau [28]. The convective heat transfer from the gas to the thermocouple was estimated assuming that the thermocouple is a cylinder placed in cross flow, with the Nusselt number of 0.5. The Reynolds number used for estimating the Nusselt number was evaluated using the wire diameters as the characteristic length, the characteristic velocity was V_2 and the kinematic viscosity was estimated at a temperature of 1500 K. The Reynolds number was 0.0055 for the uncoated thermocouple and 0.0075 for the coated thermocouple. The Prandtl number was 0.7. The heat losses from the wire by radiation were estimated assuming an emissivity of 0.2 for the uncoated wire and 0.6 for the coated wire. At the peak value of the measured temperature, the radiation correction was approximately 50 K for bare thermocouple and 100 K for the coated thermocouple. The absolute accuracy of the temperature measurement is expected to be better than ± 80 K. The flame structure of n-butanol is shown in Figs. 20 and 21 and that of iso-butanol in Figs. 23 and 24. The comparisons with predictions of the kinetic model are discussed later.

The experimental data obtained here are compared with the experimental data of Sarathy et al. [21]. The exit diameter of the fuel duct and the oxidizer duct of the counterflow burner employed in this previous study was 25.4 mm, and the separation distance $L = 20$ mm. The fuel stream was a mixture of 94.11% N₂ and 5.89% n-butanol by volume ($Y_{F,1} = 0.142$) with $T_1 = 356$ K. The mass flow rate of the fuel stream was 0.131 kg/(m² s). The oxidizer stream was a mixture of 42.25% O₂ and 57.75% N₂ by volume ($Y_{O_2,2} = 0.4554$) with $T_2 = 423$ K. The mass flow rate of the oxidizer stream was 0.126 kg/(m² s). At these conditions, the flame is on the fuel side of the stagnation plane with the stoichiometric mixture fraction $Z_{st} = 0.5528$, and the strain rate at the stagnation plane in the region between the stagnation plane and the fuel boundary was $a_1 = a_2(\rho_2/\rho_1)^{0.5} = 33$ s⁻¹. The flame structure of this n-butanol flame [21] is shown in Fig. 22.

3. Kinetic mechanism and reaction classes

Figs. 3–6 show simplified primary decomposition mechanisms for the four isomers of butanol—n-butanol, sec-butanol, iso-butanol, and tert-butanol. As shown in Fig. 3, five different radicals are formed via H-abstraction reactions from n-C₄H₉OH. Subsequently, these radicals isomerise and decompose. 1-Butene

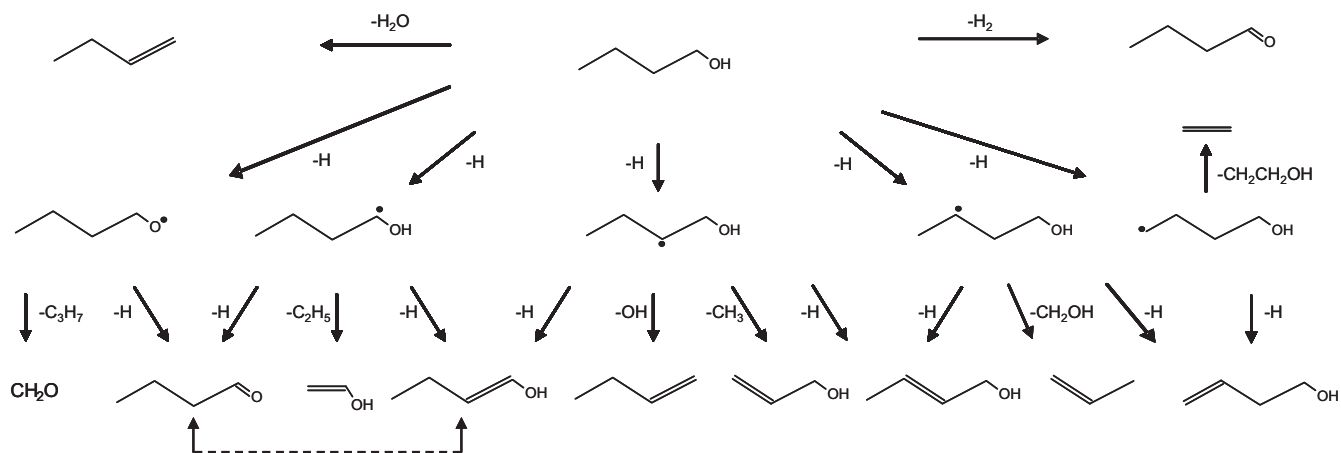


Fig. 3. Primary decomposition reactions of n-butanol.

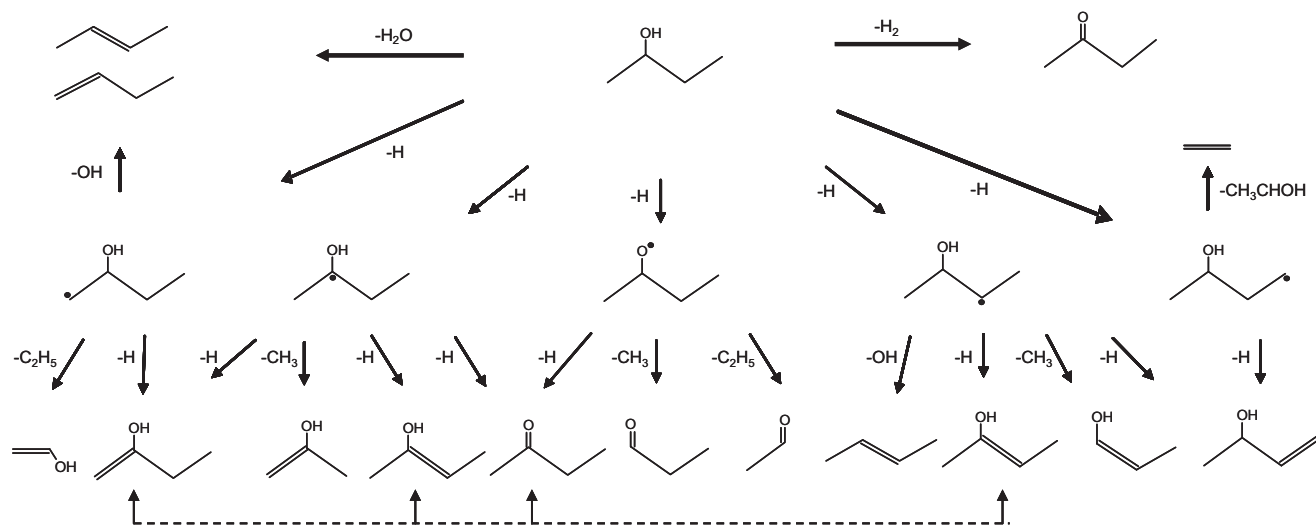


Fig. 4. Primary decomposition reactions of sec-butanol.

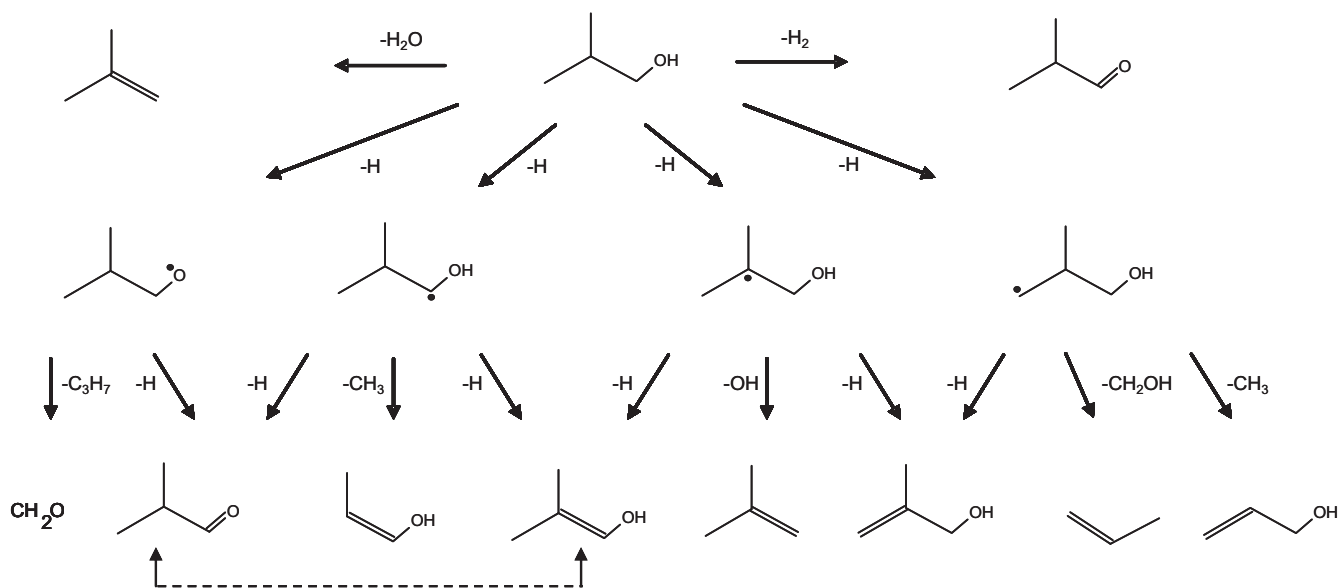


Fig. 5. Primary decomposition reactions of iso-butanol.

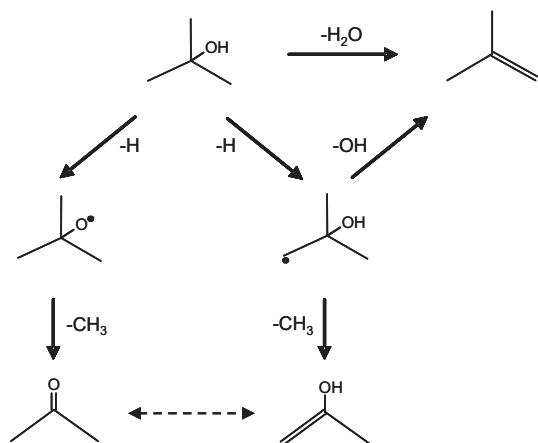


Fig. 6. Primary decomposition reactions of tert-butanol.

(1-C₄H₈) is the result of the molecular dehydration reaction as well as the dehydroxylation reaction of n-C₄H₈OH β radical. Butanal (n-C₃H₇CHO) and/or butenyl alcohols are formed from dehydrogenation reactions of all the five primary radicals. Butanal, methyl-ethyl-ketone (MEK) and methylpropanal are also formed by molecular dehydrogenation of n-butanol, sec-butanol, and iso-butanol, respectively. Allyl and vinyl alcohols are formed from β -decomposition reactions of n-C₄H₈OH α and n-C₄H₈OH β . α -Unsaturated alcohols, usually formed at high temperatures, are considered as directly transformed into the corresponding aldehydes, through the keto-enol tautomerization, which is quite fast in these conditions. This allows to reduce the total number of species in the overall kinetic scheme.

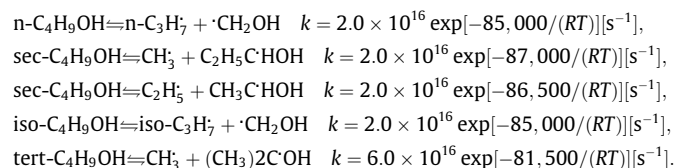
For the sake of brevity, isomerisation reactions among the primary butanol radicals are not reported in this scheme. Similarly, as shown in Fig. 4, sec-C₄H₉OH forms five different primary radicals and MEK is the fingerprint of this alcohol. Fig. 5 shows that there are four primary radicals of iso-butanol, while only two radicals are formed from tert-butanol (Fig. 6).

The pyrolysis and oxidation mechanisms of butanol isomers are similar to those for hydrocarbon fuels. Here the development of the complete set of the primary propagation reactions for butanol isomers proceeds from the extension of the kinetic parameters for similar reactions already studied and recently revised for ethanol, n-propanol and iso-propanol [1,7–15]. The kinetic study of oxidation of n-propanol and iso-propanol is a useful starting point for the extension of the kinetic scheme to butanol isomers [15]. Initiation reactions are, in general, evaluated by assuming a reference frequency factor, A, with the activation energy, E equal to the bond energy, and microscopic reversibility based on the reverse radical recombination reaction is applied. Metathesis reactions require defining the reactivity of the H atoms in hydroxyl position and the H atoms in α position. Remaining H atoms are presumed to be unaffected by the presence of the OH group. Decomposition reactions of the corresponding alkoxy and parent radicals from alcohol fuels need further elaboration. Isomerization reactions of these radicals are significant and could enhance the role of the very reactive alkoxy radical. Finally, the class of the four-center molecular dehydration reactions requires a careful and systematic discussion in order to highlight the role of primary, secondary and tertiary sites. In this section, unimolecular reactions are discussed first followed by metatheses reactions, decomposition and isomerization reactions of primary radicals from alcohol fuels, and four-center molecular dehydration reactions. The rate constant, k_i for reaction i is written as $k_i = A_i T^{n_i} \exp[-E_i/(RT)]$, where A_i is the frequency factor, E_i is the activation energy in cal/mol, T the temperature, n_i the temperature exponent, and R is the gas constant.

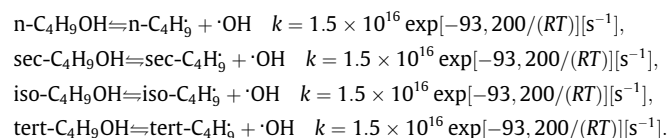
Pressure dependence is not included in these expressions. However, it is worth having a caution, as high temperatures or very low pressures are considered.

3.1. Unimolecular initiation reactions

The activation energy of initiation reactions are evaluated from the strength of the C–C bond by defining the bond energy of primary, secondary and tertiary C atoms (C_p , C_s , and C_t) with the different C atoms with OH substitution ($C(OH)_{p/s/t}$). The four butanol isomers are good examples to define and illustrate this reaction class of unimolecular initiation reactions:



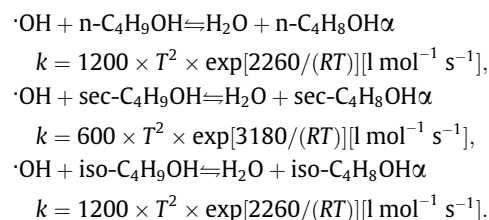
Kinetic data for the remaining initiation reactions, that involve the splitting of the C–C bond, are similar to those used for alkanes. The following kinetic parameters are prescribed for the reactions that result in formation of the OH radical:



They are the same as that for the similar propanol initiation reactions. Note that these reference kinetic parameters are not affected by the nature of the C atom. High activation energies are required to release the H atoms from the OH group or the carbon skeleton, therefore reactions of this type cannot contribute to fuel decomposition. On the contrary, the reverse reactions could affect flame propagation and all these reactions are included in the overall mechanism with the same kinetic parameter $k = 5.0 \times 10^{10} [\text{l mol}^{-1} \text{s}^{-1}]$.

3.2. Metathesis reactions

Metathesis reactions are treated according to the systematic approach described elsewhere [29]. Following the kinetic model for propanol isomers [15], the kinetic parameters for the H-atom abstraction from the alcohol functional group are assumed to be equal to those for the abstraction of a primary H atom from a methyl group. Galano et al. [30] studied the gas phase reactions of alcohols with the OH radical employing a quantum mechanical approach. Different from the previous recommended values [31,32], they concluded that the rate coefficient corresponding to the α channel (k_α) is larger than those of the other competing channels. Further considerations of Galano et al. [30] relating to the higher reactivity of the γ -site at low temperatures could be simply attributed to the higher reactivity of the ($\omega - 1$) sites and are neglected here. Similar arguments were also recently put forward by Black et al. [18]. On the basis of these previous studies, we assume the following kinetic parameters for the H-abstraction reactions of OH radicals in α position (units are: cal, l, mole, s, K):

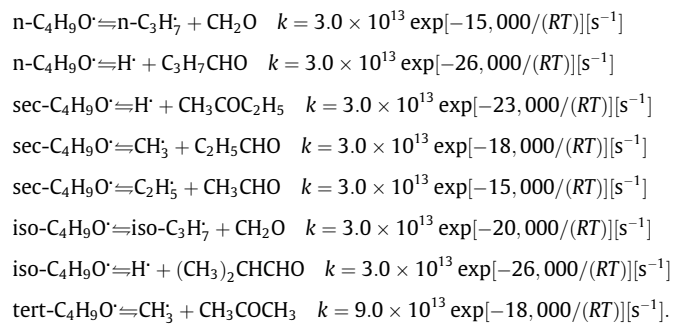


Thus, kinetic parameters of H abstractions in α position from n-butanol and iso-butanol are obtained by increasing by 50% the frequency factors of the two secondary H atoms, while the parameters for sec-butanol are obtained by increasing by 50% the frequency factor of the tertiary H atom. As an example, the selectivity of n-butanol radicals is $n\text{-C}_4\text{H}_8\text{OH}\alpha > n\text{-C}_4\text{H}_8\text{OH}\beta \approx n\text{-C}_4\text{H}_8\text{OH}\gamma > n\text{-C}_4\text{H}_8\text{OH}\delta > n\text{-C}_4\text{H}_9\text{O}$.

For the other H sites, the systematic approach for metathesis reactions, described elsewhere is maintained [29,33]. Metathesis reactions of H, CH_3 and other abstracting radicals are treated following the same approach.

3.3. Decomposition reactions of alkoxy radicals

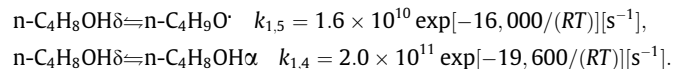
The kinetic parameters of alkoxy radicals decomposition reactions via β -scission have been recently discussed by Curran [34] and Frassoldati et al. [15]. Alkoxy radical decompositions to form alkyl radicals prevail over the dehydrogenation reaction paths. The analogy with propanol decomposition reactions suggests the use of the following kinetic parameters:



These rate expressions highlight the high reactivity of alkoxy radicals and the low selectivity toward the dehydrogenation channel. In the temperature range of 700–1000 K decomposition reactions are at least 10 times faster. Kinetic data for other decomposition and dehydrogenation reactions of alkoxy and alkyl-hydroxy radicals are the same as those used for propanol and alkane fuels.

3.4. Isomerization reactions

Isomerization reactions of primary radicals can play an important role during the first decomposition steps, mainly due to the high reactivity of butoxy radicals. In fact, 1–4 and 1–5 H transfer reactions are explained on the basis of internal H-abstraction reactions, via 5-membered and 6-membered ring intermediates. The rate constants of these isomerization reactions are estimated in terms of the number of atoms in the transition state ring structure (including the H atom) and the type of sites involved in the H transfer [35,36]. Based on similar reactions of alkyl radicals, the following isomerization reactions of n-C₄H₈OH δ are considered:



Values for the rate parameters for the isomerization reactions are obtained by using the reference kinetic parameters, accounting for the extra activation energy for the ring strain and decreasing the frequency factor for the tie up of the additional rotors [37]. Fig. 7 compares the values of rate parameters of these isomerization reactions with the β -decomposition and the dehydrogenation reaction of n-C₄H₈OH δ :

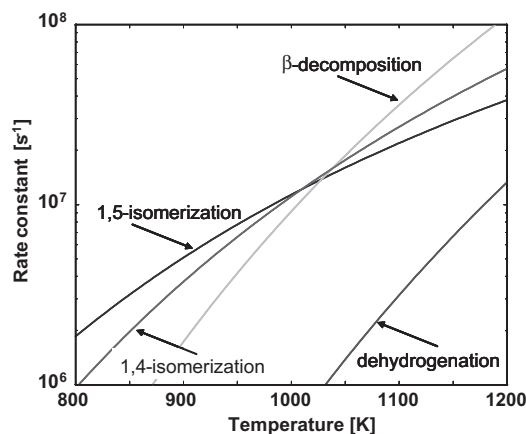
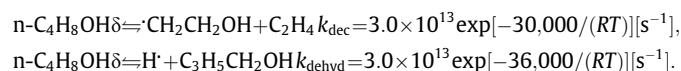


Fig. 7. Isomerization and decomposition reactions of n-C₄H₈OH δ radical.

Decomposition reactions prevail only at temperatures higher than 1000–1100 K, while the 1–5 isomerization reaction dominates at temperatures lower than 900 K. Moreover, dehydrogenation reaction could compete only at flame temperatures. Of course, these isomerization reactions are more effective when less reactive radicals form the unstable alkoxy radicals.

3.5. Four-center molecular dehydration reactions

This class of reactions involves a four-center cyclic transition state with the formation of parent alkenes and H₂O, as shown in Fig. 8. Thus sec-butanol dehydration can form either 1-butene or 2-butene, depending on the different four membered ring transition intermediate. Several kinetic parameters have been suggested for this class of reactions [9,10,16,17,38–40]. Different activation energies and frequency factors are expected depending on the type of OH and the number and the type of H involved.

Moss et al. [17] have proposed different values for the different butanol isomers. They used for iso-butanol the kinetic parameters proposed by Bui et al. [40] for iso-propanol, while the rate parameters for the other isomers were fitted in order to obtain sufficient agreement with their experimental ignition delay times. They also observed a disagreement between all the fitted rate constants and suggested the need for a better analysis of these reactions, mainly due to their large sensitivity. In order to define a general rule for this class of reactions, it is first useful to select the kinetic parameters of a reference reaction, where the dehydration involves a primary $\cdot\text{OH}$ group and a single primary H atom. On the basis of the previous kinetic studies, these reference kinetic parameters are assumed

$$k = 5.0 \times 10^{13} \exp[-68,600/(RT)] [\text{s}^{-1}]$$

The frequency factor will account for the number of H atoms while the activation energy reflects the type of H atoms and the type of OH group. A reduction of activation energy of 1000 and 3000 cal/mol is assumed for secondary and tertiary H atoms, respectively.

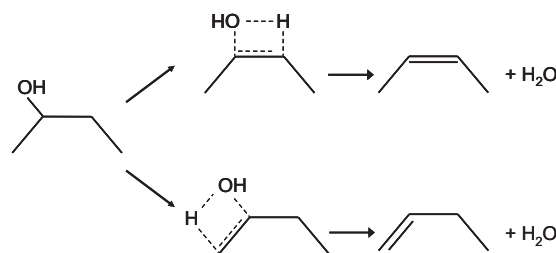
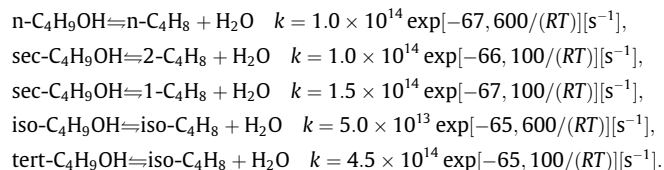


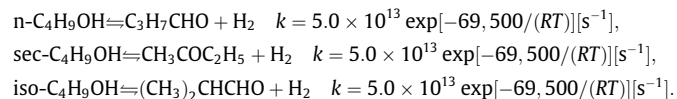
Fig. 8. Dehydration reactions of sec-butanol to form 1-butene and 2-butene.

These corrections reveal the differences in the bond energy of the released chemical bonds. According to Markovnikov's rule and the kinetic study of Dente [41] the corrections relating the type of the OH group reflect the different ionization propensity of the substituted C atoms. With the addition of a protic acid such as H–X to an alkene, the acid hydrogen (H) attaches to the C atom with the greatest number of hydrogen atoms, and the halide group (X) attaches to the more substituted C atom. Due to the analogy of H–OH additions and the microscopic reversibility of elementary reactions, corrections of 1500 and 3500 kcal/kmol are assumed when secondary and tertiary OH groups are involved in the cyclic transition state. Thus, the following kinetic parameters of the dehydration reactions are assumed for the different butanol isomers:

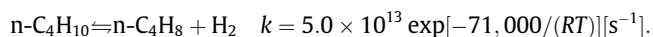


Dehydrogenation reactions are another class of four-center molecular reactions. These and similar reactions have been extensively and systematically studied by Dente [41]. Dehydrogenation reactions

directly form acyl groups and could become of interest mainly at low pressures. As an example, the following molecular dehydrogenation reactions are considered:



Due to the formation of acyl group, these reactions require lower activation energy, when compared to the corresponding ones of alkanes [42].



The detailed sub-mechanism of the four butanol isomers is reported in Table 1, together with the kinetic parameters. Further pyrolysis and/or oxidation reactions of intermediate products are described in a semi-detailed oxidation mechanism for hydrocarbon fuels up to C₁₆ developed previously [43–45]. The overall kinetic scheme is based on hierarchical modularity and is made up of more than 7000 reactions among 300 species. Thermochemical data for most species was obtained from the CHEMKIN thermodynamic database [46,47]. For those species for which thermodynamic data is not available in the literature, the group additive method was used to estimate these properties [35]. The complete mechanism, with

Table 1

Sub-mechanism of butanol isomers [units are: l, mol, s, cal].

Reactions	A	n	E
<i>n-Butanol</i>			
$n\text{C}_4\text{H}_9\text{OH} \rightleftharpoons n\text{C}_3\text{H}_7 + \cdot\text{CH}_2\text{OH}$	$2.0 \times 10^{+16}$	0	85,000
$n\text{C}_4\text{H}_9\text{OH} \rightleftharpoons \text{C}_2\text{H}_5 + \cdot\text{CH}_2\text{CH}_2\text{OH}$	$2.0 \times 10^{+16}$	0	85,000
$n\text{C}_4\text{H}_9\text{OH} \rightleftharpoons \text{CH}_3 + \cdot\text{CH}_2\text{CH}_2\text{CH}_2\text{OH}$	$2.0 \times 10^{+16}$	0	86,000
$n\text{C}_4\text{H}_9\text{OH} \rightleftharpoons \cdot\text{OH} + \cdot\text{CH}_2\text{CH}_2\text{CH}_2\text{CH}_3$	$1.5 \times 10^{+16}$	0	93,200
$n\text{C}_4\text{H}_8\text{OH}\alpha + \text{H}\cdot \rightleftharpoons n\text{C}_4\text{H}_9\text{OH}$	$5.0 \times 10^{+10}$	0	0
$n\text{C}_4\text{H}_8\text{OH}\beta + \text{H}\cdot \rightleftharpoons n\text{C}_4\text{H}_9\text{OH}$	$5.0 \times 10^{+10}$	0	0
$n\text{C}_4\text{H}_8\text{OH}\gamma + \text{H}\cdot \rightleftharpoons n\text{C}_4\text{H}_9\text{OH}$	$5.0 \times 10^{+10}$	0	0
$n\text{C}_4\text{H}_8\text{OH}\delta + \text{H}\cdot \rightleftharpoons n\text{C}_4\text{H}_9\text{OH}$	$5.0 \times 10^{+10}$	0	0
$n\text{C}_4\text{H}_9\text{O} + \text{H}\cdot \rightleftharpoons n\text{C}_4\text{H}_9\text{OH}$	$5.0 \times 10^{+10}$	0	0
$n\text{C}_4\text{H}_9\text{OH} \rightleftharpoons \text{H}_2\text{O} + n\text{C}_4\text{H}_8$	$1.0 \times 10^{+14}$	0	67,600
$n\text{C}_4\text{H}_9\text{OH} \rightleftharpoons \text{H}_2 + \text{C}_3\text{H}_7\text{CHO}$	$5.0 \times 10^{+13}$	0	69,500
$\text{R} + n\text{C}_4\text{H}_9\text{OH} \rightarrow \text{RH} + n\text{C}_4\text{H}_8\text{OH}\alpha$	$3\text{H}_{\text{Secondary}}^{\text{a}}$		
$\text{R} + n\text{C}_4\text{H}_9\text{OH} \rightarrow \text{RH} + n\text{C}_4\text{H}_8\text{OH}\beta$	$2\text{H}_{\text{Secondary}}^{\text{a}}$		
$\text{R} + n\text{C}_4\text{H}_9\text{OH} \rightarrow \text{RH} + n\text{C}_4\text{H}_8\text{OH}\gamma$	$2\text{H}_{\text{Secondary}}^{\text{a}}$		
$\text{R} + n\text{C}_4\text{H}_9\text{OH} \rightarrow \text{RH} + n\text{C}_4\text{H}_8\text{OH}\delta$	$3\text{H}_{\text{Primary}}^{\text{a}}$		
$\text{R} + n\text{C}_4\text{H}_9\text{OH} \rightarrow \text{RH} + n\text{C}_4\text{H}_9\text{O}$	$1\text{H}_{\text{Primary}}^{\text{a}}$		
$n\text{C}_4\text{H}_8\text{OH}\alpha \rightleftharpoons \text{C}_2\text{H}_5 + \text{CH}_3\text{CHO}$	$3.0 \times 10^{+13}$	0	31,000
$n\text{C}_4\text{H}_8\text{OH}\alpha \rightleftharpoons \text{H}\cdot + \text{C}_3\text{H}_7\text{CHO}$	$3.0 \times 10^{+13}$	0	37,000
$n\text{C}_4\text{H}_8\text{OH}\beta \rightleftharpoons \cdot\text{OH} + n\text{C}_4\text{H}_8$	$3.0 \times 10^{+13}$	0	33,000
$n\text{C}_4\text{H}_8\text{OH}\beta \rightleftharpoons \text{CH}_3 + \text{C}_2\text{H}_5\text{CHO}$	$3.0 \times 10^{+13}$	0	34,000
$n\text{C}_4\text{H}_8\text{OH}\beta \rightleftharpoons \text{H}\cdot + \text{C}_3\text{H}_7\text{CHO}$	$3.0 \times 10^{+13}$	0	37,000
$n\text{C}_4\text{H}_8\text{OH}\gamma \rightleftharpoons \text{H}\cdot + \text{C}_4\text{H}_7\text{OH}$	$3.0 \times 10^{+13}$	0	37,000
$n\text{C}_4\text{H}_8\text{OH}\gamma \rightleftharpoons \cdot\text{CH}_2\text{OH} + \text{C}_3\text{H}_6$	$3.0 \times 10^{+13}$	0	30,000
$n\text{C}_4\text{H}_8\text{OH}\delta \rightleftharpoons \cdot\text{H} + \text{C}_4\text{H}_7\text{OH}$	$3.0 \times 10^{+13}$	0	36,000
$n\text{C}_4\text{H}_8\text{OH}\delta \rightleftharpoons \cdot\text{CH}_2\text{CH}_2\text{OH} + \text{C}_2\text{H}_4$	$3.0 \times 10^{+13}$	0	30,000
$n\text{C}_4\text{H}_9\text{O} \rightleftharpoons \text{H}\cdot + \text{C}_3\text{H}_7\text{CHO}$	$3.0 \times 10^{+13}$	0	26,000
$n\text{C}_4\text{H}_9\text{O} \rightleftharpoons 1 - \text{C}_3\text{H}_7 + \text{CH}_2\text{O}$	$3.0 \times 10^{+13}$	0	15,000
$n\text{C}_4\text{H}_8\text{OH}\delta \rightleftharpoons n\text{C}_4\text{H}_9\text{O}$	$1.6 \times 10^{+10}$	0	16,000
$n\text{C}_4\text{H}_8\text{OH}\delta \rightleftharpoons n\text{C}_4\text{H}_8\text{OH}\alpha$	$2.0 \times 10^{+11}$	0	19,600
$n\text{C}_4\text{H}_8\text{OH}\gamma \rightleftharpoons n\text{C}_4\text{H}_9\text{O}$	$1.0 \times 10^{+11}$	0	23,000
$\text{O}_2 + n\text{C}_4\text{H}_8\text{OH}\alpha \rightleftharpoons \text{HO}_2 + \text{C}_3\text{H}_7\text{CHO}$	$1.5 \times 10^{+9}$	0	3500
$\text{O}_2 + n\text{C}_4\text{H}_8\text{OH}\beta \rightleftharpoons \text{HO}_2 + 0.67\text{C}_3\text{H}_7\text{CHO} + 0.33\text{C}_4\text{H}_7\text{OH}$	$1.5 \times 10^{+9}$	0	3500
$\text{O}_2 + n\text{C}_4\text{H}_8\text{OH}\gamma \rightleftharpoons \text{HO}_2 + \text{C}_4\text{H}_7\text{OH}$	$1.5 \times 10^{+9}$	0	3500
$\text{O}_2 + n\text{C}_4\text{H}_8\text{OH}\delta \rightleftharpoons \text{HO}_2 + \text{C}_4\text{H}_7\text{OH}$	$1.5 \times 10^{+9}$	0	3500
$\text{O}_2 + n\text{C}_4\text{H}_9\text{O} \rightleftharpoons \text{HO}_2 + \text{C}_3\text{H}_7\text{CHO}$	$1.5 \times 10^{+9}$	0	3500
<i>sec-Butanol</i>			
$s\text{C}_4\text{H}_9\text{OH} \rightleftharpoons \text{C}_2\text{H}_5 + \text{CH}_2\text{CH}\cdot\text{OH}$	$2.0 \times 10^{+16}$	0	86,500
$s\text{C}_4\text{H}_9\text{OH} \rightleftharpoons \text{CH}_3 + \cdot\text{CHOHCH}_2\text{CH}_3$	$2.0 \times 10^{+16}$	0	87,000
$s\text{C}_4\text{H}_9\text{OH} \rightleftharpoons \text{CH}_3 + \cdot\text{CH}_2\text{CH}_2\text{CH}_2\text{OH}$	$2.0 \times 10^{+16}$	0	87,000
$s\text{C}_4\text{H}_9\text{OH} \rightleftharpoons \cdot\text{OH} + \cdot\text{CH}_2\text{CH}_2\text{CH}_2\text{CH}_3$	$1.5 \times 10^{+16}$	0	93,200
$s\text{C}_4\text{H}_8\text{OH}\alpha + \text{H}\cdot \rightleftharpoons s\text{C}_4\text{H}_9\text{OH}$	$5.0 \times 10^{+10}$	0	0

(continued on next page)

Table 1 (continued)

Reactions	A	n	E
$sC_4H_8OH\beta s + H \rightleftharpoons sC_4H_9OH$	$5.0 \times 10^{+10}$	0	0
$sC_4H_8OH\beta p + H \rightleftharpoons sC_4H_9OH$	$5.0 \times 10^{+10}$	0	0
$sC_4H_8OH\gamma + H \rightleftharpoons sC_4H_9OH$	$5.0 \times 10^{+10}$	0	0
$sC_4H_9O + H \rightleftharpoons sC_4H_9OH$	$5.0 \times 10^{+10}$	0	0
$sC_4H_9OH \rightleftharpoons H_2O + 1C_4H_8$	$1.5 \times 10^{+14}$	0	67,100
$sC_4H_9OH \rightleftharpoons H_2O + 2C_4H_8$	$1.0 \times 10^{+14}$	0	66,100
$sC_4H_9OH \rightleftharpoons H_2 + CH_3COC_2H_5$	$5.0 \times 10^{+13}$	0	69,500
$R + sC_4H_9OH \rightarrow RH + sC_4H_8OH\alpha$	$1.5H_{Tertiary}^a$		
$R + sC_4H_9OH \rightarrow RH + sC_4H_8OH\beta p$	$3H_{Primary}^a$		
$R + sC_4H_9OH \rightarrow RH + sC_4H_8OH\beta s$	$2H_{Secondary}^a$		
$R + sC_4H_9OH \rightarrow RH + sC_4H_8OH\gamma$	$3H_{Primary}^a$		
$R + sC_4H_9OH \rightarrow RH + sC_4H_9O$	$1H_{Primary}^a$		
$sC_4H_8OH\alpha \rightleftharpoons CH_3 + (CH_3)_2CO$	$3.0 \times 10^{+13}$	0	32,000
$sC_4H_8OH\alpha \rightleftharpoons H + CH_3COC_2H_5$	$3.0 \times 10^{+13}$	0	37,000
$sC_4H_8OH\beta p \rightleftharpoons C_2H_5 + CH_3CHO$	$3.0 \times 10^{+13}$	0	30,000
$sC_4H_8OH\beta p \rightleftharpoons H + CH_3COC_2H_5$	$3.0 \times 10^{+13}$	0	37,000
$sC_4H_8OH\beta p \rightleftharpoons \cdot OH + C_4H_8$	$3.0 \times 10^{+13}$	0	35,000
$sC_4H_8OH\beta s \rightleftharpoons CH_3 + C_3H_7CHO$	$3.0 \times 10^{+13}$	0	32,000
$sC_4H_8OH\beta s \rightleftharpoons H + CH_3COC_2H_5$	$3.0 \times 10^{+13}$	0	37,000
$sC_4H_8OH\beta s \rightleftharpoons H + C_4H_7OH$	$3.0 \times 10^{+13}$	0	37,000
$sC_4H_8OH\beta s \rightleftharpoons \cdot OH + C_4H_8$	$3.0 \times 10^{+13}$	0	26,000
$sC_4H_8OH\gamma \rightleftharpoons H + C_4H_7OH$	$3.0 \times 10^{+13}$	0	37,000
$sC_4H_8OH\gamma \rightleftharpoons CH_2CH\cdot OH + C_2H_4$	$3.0 \times 10^{+13}$	0	30,000
$sC_4H_9O \rightleftharpoons CH_3 + C_3H_7CHO$	$3.0 \times 10^{+13}$	0	18,000
$sC_4H_9O \rightleftharpoons C_2H_5 + CH_3CHO$	$3.0 \times 10^{+13}$	0	15,000
$sC_4H_9O \rightleftharpoons H + CH_3COC_2H_5$	$3.0 \times 10^{+13}$	0	23,000
$sC_4H_8OH\gamma \rightleftharpoons sC_4H_9O$	$1.0 \times 10^{+11}$	0	21,000
$sC_4H_8OH\gamma \rightleftharpoons sC_4H_8OH\beta p$	$3.0 \times 10^{+11}$	0	19,500
$O_2 + sC_4H_8OH\alpha \rightleftharpoons HO_2 + CH_3COC_2H_5$	$1.5 \times 10^{+9}$	0	3500
$O_2 + sC_4H_8OH\beta p \rightleftharpoons HO_2 + CH_3COC_2H_5$	$1.5 \times 10^{+9}$	0	3500
$O_2 + sC_4H_8OH\beta s \rightleftharpoons HO_2 + 0.67CH_3COC_2H_5 + 0.33C_4H_7OH$	$1.5 \times 10^{+9}$	0	3500
$O_2 + C_4H_8OH\gamma \rightleftharpoons HO_2 + C_4H_7OH$	$1.5 \times 10^{+9}$	0	3500
$O_2 + sC_4H_9O \rightleftharpoons HO_2 + CH_3COC_2H_5$	$1.5 \times 10^{+9}$	0	3500
<i>iso-Butanol</i>			
$iC_4H_9OH \rightleftharpoons iC_3H_7 + \cdot CH_2OH$	$2.0 \times 10^{+16}$	0	85,000
$iC_4H_9OH \rightleftharpoons CH_3 + CH_3CHCH_2OH$	$2.0 \times 10^{+16}$	0	88,000
$iC_4H_9OH \rightleftharpoons \cdot OH + (CH_3)_2CH\cdot CH_2$	$1.5 \times 10^{+16}$	0	93,200
$iC_4H_8OH\alpha + H \rightleftharpoons iC_4H_9OH$	$5.0 \times 10^{+10}$	0	0
$iC_4H_8OH\beta + H \rightleftharpoons iC_4H_9OH$	$5.0 \times 10^{+10}$	0	0
$iC_4H_8OH\gamma + H \rightleftharpoons iC_4H_9OH$	$5.0 \times 10^{+10}$	0	0
$iC_4H_9O + H \rightleftharpoons iC_4H_9OH$	$5.0 \times 10^{+10}$	0	0
$iC_4H_9OH \rightleftharpoons H_2O + i - C_4H_8$	$5.0 \times 10^{+13}$	0	65,600
$iC_4H_9OH \rightleftharpoons H_2 + (CH_3)_2CHCHO$	$5.0 \times 10^{+13}$	0	69,500
$R + iC_4H_9OH \rightarrow RH + iC_4H_8OH\alpha$	$3H_{Secondary}^a$		
$R + iC_4H_9OH \rightarrow RH + iC_4H_8OH\beta$	$1H_{Tertiary}^a$		
$R + iC_4H_9OH \rightarrow RH + iC_4H_8OH\gamma$	$6H_{Primary}^a$		
$R + iC_4H_9OH \rightarrow RH + iC_4H_9O$	$1H_{Primary}^a$		
$iC_4H_8OH\alpha \rightleftharpoons CH_3 + C_3H_7CHO$	$3.0 \times 10^{+13}$	0	32,000
$iC_4H_8OH\alpha \rightleftharpoons H + (CH_3)_2CHCHO$	$3.0 \times 10^{+13}$	0	37,000
$iC_4H_8OH\beta \rightleftharpoons \cdot OH + i - C_4H_8$	$3.0 \times 10^{+13}$	0	36,000
$iC_4H_8OH\beta \rightleftharpoons H + C_4H_7OH$	$3.0 \times 10^{+13}$	0	37,000
$iC_4H_8OH\beta \rightleftharpoons H + (CH_3)_2CHCHO$	$3.0 \times 10^{+13}$	0	37,000
$iC_4H_8OH\gamma \rightleftharpoons CH_3 + C_3H_7CHO$	$3.0 \times 10^{+13}$	0	32,000
$iC_4H_8OH\gamma \rightleftharpoons \cdot CH_2OH + C_3H_6$	$3.0 \times 10^{+13}$	0	32,000
$iC_4H_8OH\gamma \rightleftharpoons H + C_4H_7OH$	$3.0 \times 10^{+13}$	0	37,000
$iC_4H_9O \rightarrow CH_2O + i - C_3H_6$	$3.0 \times 10^{+13}$	0	20,000
$iC_4H_9O \rightarrow H + (CH_3)_2CHCHO$	$3.0 \times 10^{+13}$	0	26,000
$iC_4H_8OH\gamma \rightleftharpoons iC_4H_9O$	$1.0 \times 10^{+11}$	0	21,500
$O_2 + iC_4H_8OH\alpha \rightleftharpoons HO_2 + (CH_3)_2CHCHO$	$1.5 \times 10^{+9}$	0	3500
$O_2 + iC_4H_8OH\beta \rightleftharpoons HO_2 + 0.33(CH_3)_2CHCHO + 0.67C_4H_7OH$	$1.5 \times 10^{+9}$	0	3500
$O_2 + iC_4H_8OH\gamma \rightleftharpoons HO_2 + C_4H_7OH$	$1.5 \times 10^{+9}$	0	3500
$O_2 + iC_4H_9O \rightleftharpoons HO_2 + (CH_3)_2CHCHO$	$1.5 \times 10^{+9}$	0	3500
<i>tert-Butanol</i>			
$tC_4H_9OH \rightleftharpoons CH_3 + (CH_3)_2COH$	$6.0 \times 10^{+16}$	0	81,500
$tC_4H_9OH \rightleftharpoons \cdot OH + (CH_3)_3C$	$1.5 \times 10^{+16}$	0	93,200
$tC_4H_8OH\beta + H \rightleftharpoons tC_4H_9OH$	$5.0 \times 10^{+10}$	0	0
$tC_4H_9O + H \rightleftharpoons tC_4H_9OH$	$5.0 \times 10^{+10}$	0	0
$tC_4H_9OH \rightleftharpoons H_2O + i - C_4H_8$	$4.5 \times 10^{+14}$	0	65,100
$R + tC_4H_9OH \rightarrow RH + tC_4H_8OH\beta$	$9H_{Primary}^a$		
$R + tC_4H_9OH \rightarrow RH + tC_4H_9O$	$1H_{Primary}^a$		
$tC_4H_8OH\beta \rightleftharpoons CH_3 + (CH_3)_2CO$	$3.0 \times 10^{+13}$	0	33,000
$tC_4H_9O\beta \rightleftharpoons \cdot OH + i - C_4H_8$	$3.0 \times 10^{+13}$	0	37,000
$tC_4H_9O \rightleftharpoons CH_3 + (CH_3)_2CO$	$9.0 \times 10^{+13}$	0	18,000

^a Kinetic parameters of H-abstraction reactions are discussed in Section 3.2.

thermodynamic and transport properties, is available in CHEMKIN format [48].

4. Numerical methods and simulations

The kinetic model described in the previous section was validated by comparing the results of numerical simulations with new and previous experimental data obtained employing shock tubes, batch reactor, jet-stirred reactor and flow reactor, and counterflow non-premixed flames. The DSMOKE code was used to integrate numerically the system of differential equations that describe various aspects of combustion in shock tube and the reactors [49]. To predict aspects of combustion that include molecular transport and chemical reactions, a one dimensional laminar flame model was employed. A detailed description of this code is given elsewhere [50]. This code includes multicomponent diffusion and thermal diffusion. Discretization of the differential equations is carried out using conventional finite differencing techniques for non-uniform mesh spacing. The numerical problem corresponds to a large system of differential–algebraic equations (DAE). The specifically conceived methods and solver routines of BzzMathLibrary [51,52] are used to handle the complexity of this numerical problem.

5. Model predictions and comparisons with experimental data

Validation of the kinetic mechanism was carried out over a wide range by comparing predictions with experimental data obtained:

(1) in batch reactors [53–55] and shock tubes [56] (Fig. 9),

(2) in a flow reactor [1] (Fig. 10),

(3) in a jet-stirred reactor at 1 atm and 10 atm [21,57] (Figs. 11 and 12),

(4) ignition delay times measured in shock tubes [17,18] (Figs. 13–17),

(5) new (Figs. 20 and 21) and previous [21] (Fig. 22) measurements of structures of n-butanol counterflow non-premixed flames and

(6) new measurements of structure and species profiles of iso-butanol counterflow non-premixed flames (Figs. 23 and 24).

In Figs. 9–17 and 20–26, the symbols represent experimental data and the lines are results of numerical simulations. The key features of these simulations and comparisons with experimental data are described in the following sections.

5.1. Pyrolysis experiments in batch reactors and shock tubes

Early pyrolysis and oxidation experimental and modeling studies were limited to n-butanol and tert-butanol [53–55]. These studies contributed to the discussion on the role of molecular and radical reactions in tert-butanol and n-butanol decomposition. The thermal decompositions of tert-butanol was investigated by Schultz and Kistiakowsky [53], at low pressures in a static reactor, in the temperature region of 760–830 K. Similar pyrolysis experiments both with n-butanol and tert-butanol were conducted by Barnard [54,55]. An overall decomposition rate of $k = 1.5 \times 10^{12} \exp[-56,700/(RT)]$ [s⁻¹] was obtained for n-butanol and $k = 3.1 \times 10^{11} \exp[-54,500/(RT)]$ [s⁻¹] for tert-butanol. These

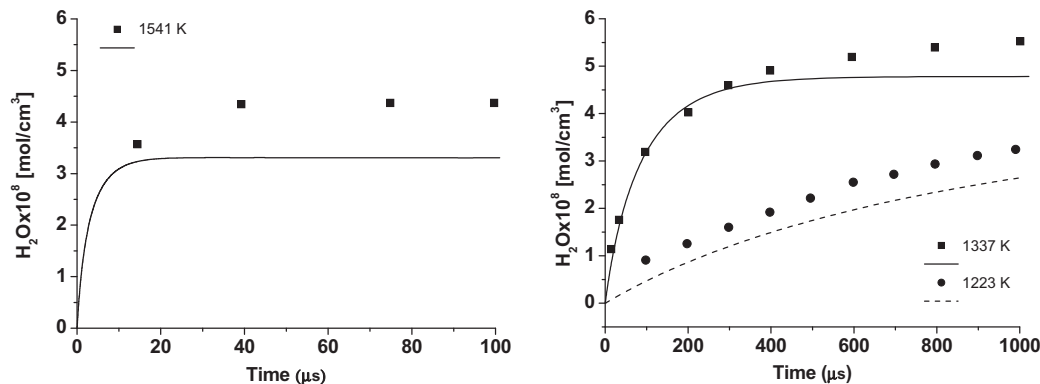


Fig. 9. Predicted and experimental concentration profiles from shock tube pyrolysis of 0.7% tert-butanol in Ar at 0.7–1 atm [56].

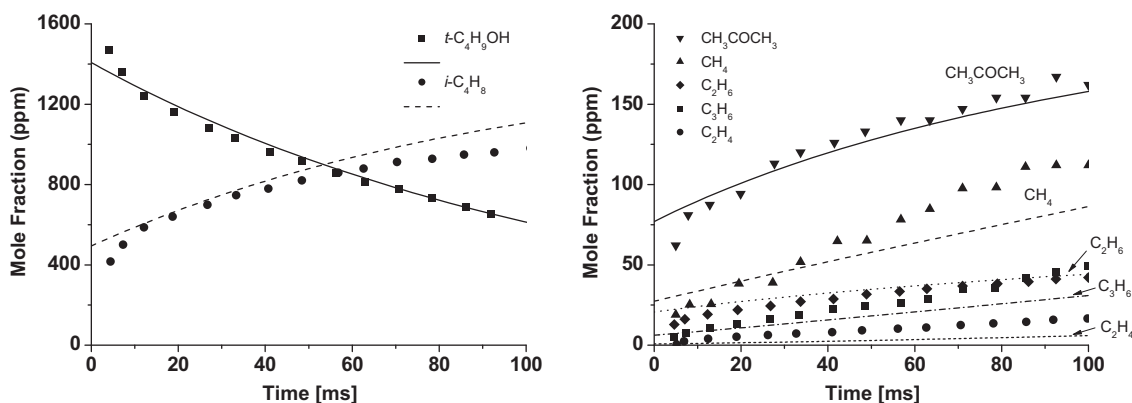


Fig. 10. Predicted and experimental concentration profiles from oxidation of 2000 ppm of tert-butanol in a flow reactor at 1 atm, $T = 1027$ K and $\phi = 0.67$ [1]. Model predictions are shifted by -25 ms.

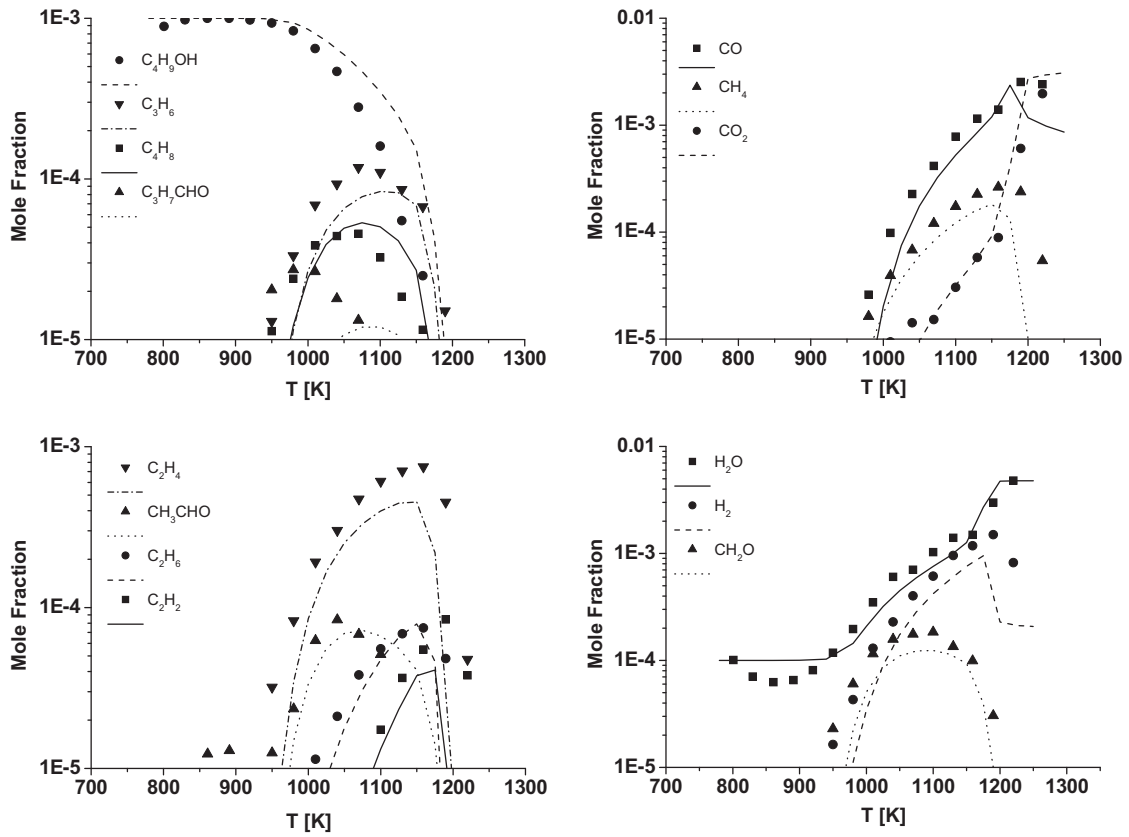


Fig. 11. Predicted and experimental concentration profiles from the oxidation of 1000 ppm of n-butanol in a JSR at 1 atm, $\Phi = 1$ and $\tau = 0.07$ s [21].

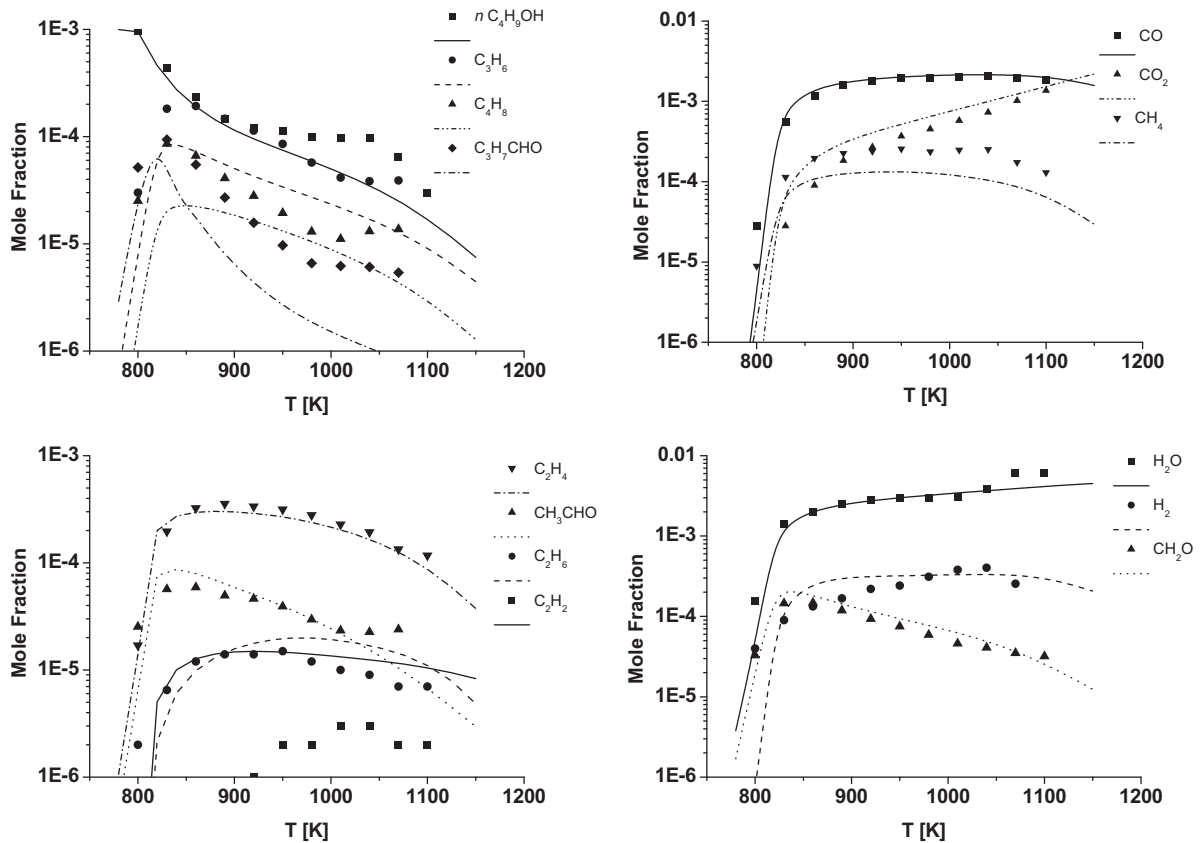


Fig. 12. Predicted and experimental concentration profiles from the oxidation of 1000 ppm of n-butanol in a JSR at 10 atm, $\Phi = 1$ and $\tau = 0.7$ s [57].

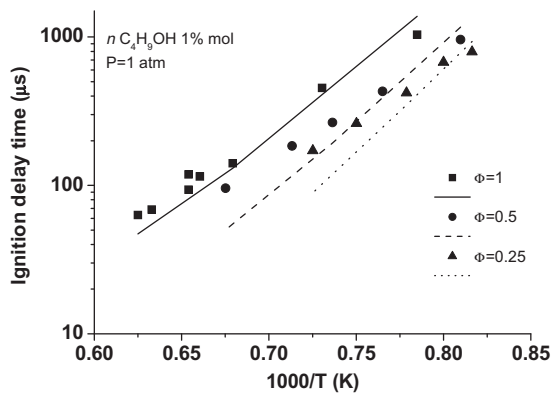


Fig. 13. Predicted and experimental ignition delay times of Ar/O₂ mixtures containing 1% n-butanol [17].

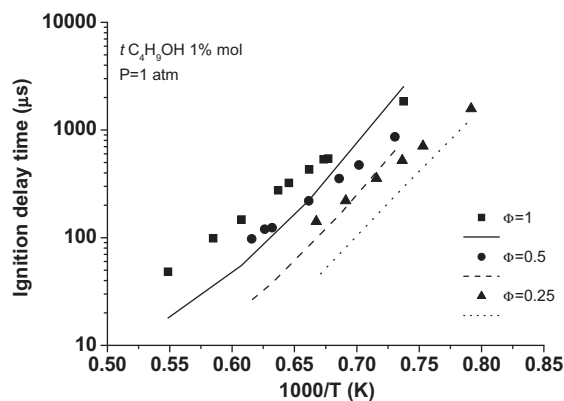


Fig. 16. Predicted and experimental ignition delay times of Ar/O₂ mixtures containing 1% tert-butanol [17].

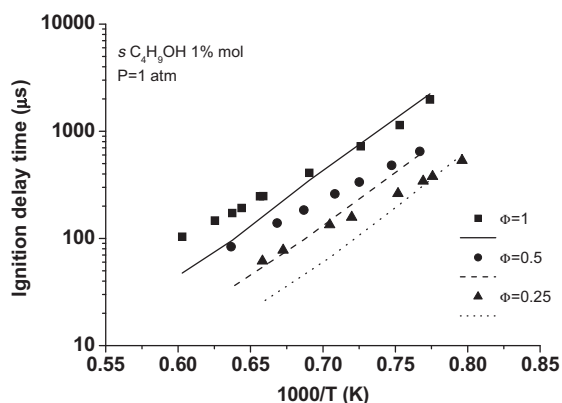


Fig. 14. Predicted and experimental ignition delay times of Ar/O₂ mixtures containing 1% sec-butanol [17].

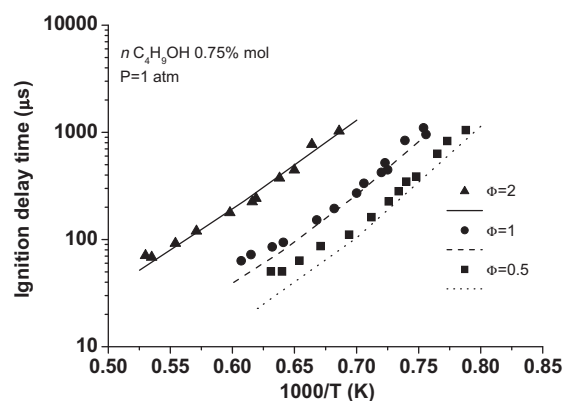


Fig. 17. Predicted and experimental ignition delay times of Ar/O₂ mixtures containing 0.75% n-butanol [18].

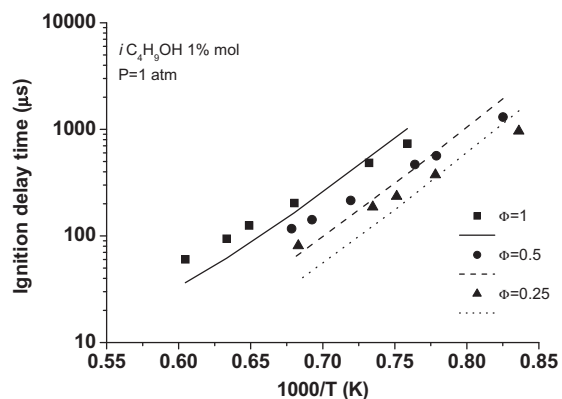


Fig. 15. Predicted and experimental ignition delay times of Ar/O₂ mixtures containing 1% iso-butanol [17].

activation energies clearly indicate the relevant role of the chain radical mechanism. In fact, while the molecular dehydration process requires around 65,000 cal/mol for both the alcohols, the apparent activation energy of the pure radical process is expected to be in the range of around 55,000 cal/mol. Model predictions of the pyrolysis of n-butanol show that more than 90% of decomposition occurs through the radical path, confirming the activation energy observed by Barnard [54]. On the contrary, similar simulations of tert-butanol pyrolysis indicate the prevailing role of the molecular dehydration while the radical path is limited to less than 25%.

Thus, the predicted activation energy should be about 64,000 cal/mol in line with the molecular reaction and in agreement with the experimental value $k = 4.8 \times 10^{14} \exp[-65,500/(RT)]$ [s⁻¹] proposed by Schultz and Kistiakowsky [53]. Pyrolysis experiments of tert-butanol at high temperatures (1200–1600 K) were reported by Choudhury et al. [56]. Fig. 9 shows the profiles of H₂O that is formed from the pyrolysis process at 1223 K, 1337 K and 1541 K. Dehydration reaction is dominant, at about 90% at 1300 K and about 70% at 1600 K. The unimolecular radical initiation reactions with high activation energy can only prevail at the high flame temperatures.

5.2. Atmospheric pressure flow reactor

Norton and Dryer [1] show experimental results for oxidation of tert-butanol in a flow reactor and a complete analysis of the oxidation of lighter alcohols. The oxidation of tert-butanol was conducted at atmospheric pressure in the Princeton flow reactor at temperatures of 1027 K and residence times of approximately 0.1 s, in lean condition ($\phi = 0.67$) and high N₂ dilution. Fig. 10 compares predictions of the kinetic model described here with experimental data of tert-butanol. Note that, following usual practice employed for comparison with flow reactor data [15], predicted profiles are shifted by -25 ms in order to match the fuel conversion. This approach and similar corrections, due to non-ideal reactant mixing and/or catalytic effects, were discussed and verified both numerically and experimentally in the literature [58]. The predictions agree well with experimental data for all species

except methane. Predictions of concentrations of CH_4 are slightly lower than the measurements. At the conditions investigated here, more than 80% of tert-butanol decomposition is attributed to the molecular dehydration reaction. The major product is iso-butene (iso- C_4H_8). Acetone ($\text{C}_3\text{H}_6\text{O}$) is the primary product of the radical decomposition path. Propene is mainly derived from the H addition reaction on iso-butene with the successive demethylation of the primary iso-butyl radical. The present kinetic model is not able to properly predict the insignificant formation of carbon monoxide and carbon dioxide. Model predictions of CO are lower than the measurements by more than a factor of five. An initial presence of CO_2 observed in the experiments could be attributed to the impurity in the reactants. It is difficult, however, to explain the formation of more than 100 ppm of CO, mainly due to the limited importance of the radical oxidation path. A delay in CO formation was also observed previously in an acetone flame [59]. This deviation could suggest that the decomposition of acetone might directly occur with a “roaming methyl” with a possible molecular path [60]. Thus, $\text{CH}_3\text{COCH}_3 \rightleftharpoons \text{C}_2\text{H}_6 + \text{CO}$. These deviations require a more complete kinetic analysis and further experimental confirmation.

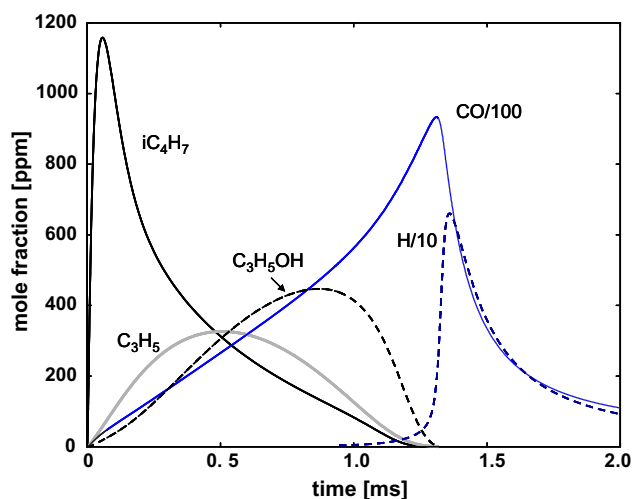


Fig. 18. Predicted values of mole fraction of intermediate species as a function of time for oxidation of a stoichiometric mixture of tert-butanol and air at 1400 K and pressure of 1 bar.

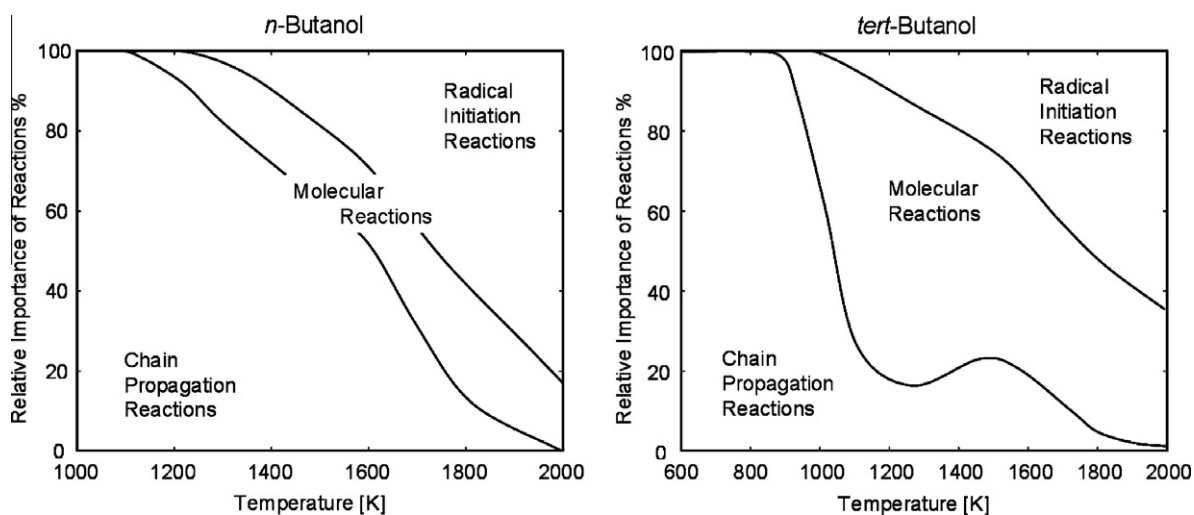


Fig. 19. Relative importance of the different reactions paths of n-butanol and tert-butanol decomposition.

5.3. n-Butanol oxidation in a jet-stirred reactor at 1 atm and 10 atm

Dagaut and coworkers studied the oxidation of n-butanol in a jet-stirred reactor with different equivalence ratios, both at 1 atm [21] and 10 atm [57].

Detailed information on the profiles of several intermediates together with CO , CO_2 and H_2O were presented. These experimental data were used to validate a detailed kinetic model for n-butanol oxidation. Figs. 11 and 12 show comparison of predictions of the kinetic model developed here with previous experimental data obtained at 1 atm [21] and 10 atm [57], respectively. Similar comparisons with the experiments at 10 atm were recently discussed also by Black et al. [18]. Figs. 11 and 12 show that the predicted reactivity of the system is somewhat lower at 1 atm, while a better agreement is observed at 10 atm. Predictions of propene and methane are slightly lower suggesting the possible greater influence of γ -butanol and β -butanol radicals, respectively. Similar deviations, at 10 atm, were also observed by Black et al. [18]. It is noteworthy that the C balance on the experimental data seems to indicate a systematic overprediction of 5–10%, even if the balance is limited to the reported/monitored species. This overprediction will be further increased if the presence of other species, such as enols, ketene and other minor intermediates is taken into account. A better agreement should be obtained by normalizing and correcting the experimental information for these systematic deviations. Similar comparisons between experimental data and model predictions are also obtained by varying the equivalence ratio, both at 1 and 10 atm.

5.4. Ignition delay times in shock tube

The high temperature autoignition of the four isomers of butanol have been experimentally studied at atmospheric pressure in a shock tube and a detailed kinetic mechanism for description of the high-temperature oxidation of butanol isomers was also discussed [17]. Ignition delay time were obtained by extrapolating the maximum slope in OH emission to the zero value and also by measuring sidewall pressure. This study facilitates comparison of the differences in combustion characteristics of the isomers. The results show that n-butanol is the most reactive and tert-butanol the least reactive [17].

The kinetic model developed here is used to predict the ignition delay times. The very sharp CH maximum is used to evaluate the ignition delay times in simulations. Figs. 13–16 compare the

predictions of ignition delay times, τ [μs] as a function of $1000/T$, with experimental data for all the four isomers. Here T is the initial temperature of the reactive mixture. The experiments and numerical simulations were performed for values of equivalence ratio, Φ , equal to 0.25, 0.5 and 1.0 with the fuel mass fraction in the reactive mixture of 0.01. The predictions of the kinetic model agree with experimental data at low temperatures. Larger deviations between predictions and data are mainly observed at temperatures higher than 1700 K.

Similar ignition delay times, limited to n-butanol oxidation, were also presented by Black et al. [18], with a detailed kinetic discussion. The data was obtained at atmospheric pressure and equivalence ratios of 0.5, 1 and 2 with the fuel mass fraction in the

reactive mixture 0.0075. Fig. 17 compares predictions of the kinetic model with experimental data. The apparent activation energies predicted are in the order of 45–50 kcal/mol, while those calculated using the measured data seem systematically lower. Similar deviations were also observed in the previous study on combustion of propanol isomers [15]. This fact clearly points to further experimental and kinetic modeling analysis.

tert-Butanol decomposes to iso-butene (iso- C_4H_8) in very short times (0.1 ms). iso-Butene is the main contributor to the overall ignition delay time. In fact, the important H-abstraction reactions on iso- C_4H_8 forms the resonantly stabilized methyl-allyl radical (iso- C_4H_7). The major decomposition reaction of iso- C_4H_7 leads to formation of propadiene (C_3H_4) and methyl radical (CH_3). Thus,

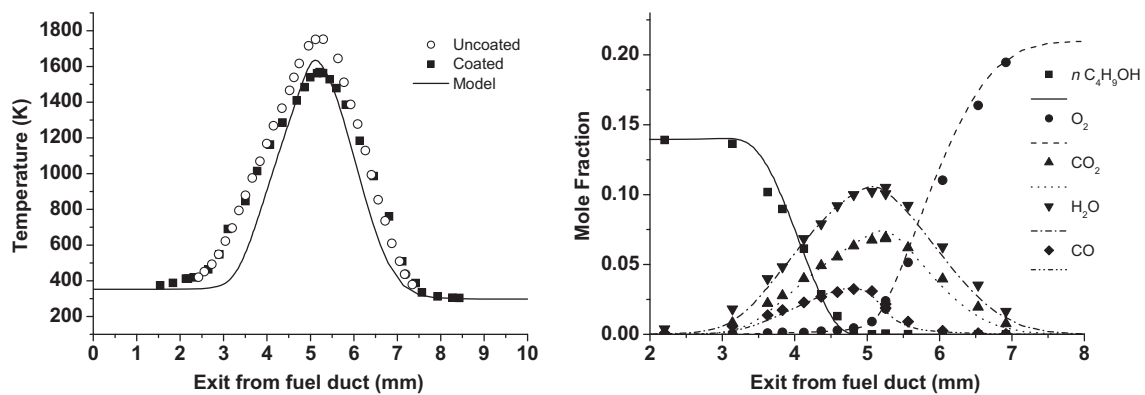


Fig. 20. Profile of temperature, and profiles of mole fraction of reactants, final products, and carbon monoxide as a function of distance from the fuel boundary for non-premixed n-butanol flame. The strain rate $a_2 = 100 \text{ s}^{-1}$, and the stoichiometric mixture fraction $Z_{\text{st}} = 0.23$. The figure shows temperature profiles, measured using bare thermocouple and coated thermocouple, and corrected to account for radiative heat losses from the wire.

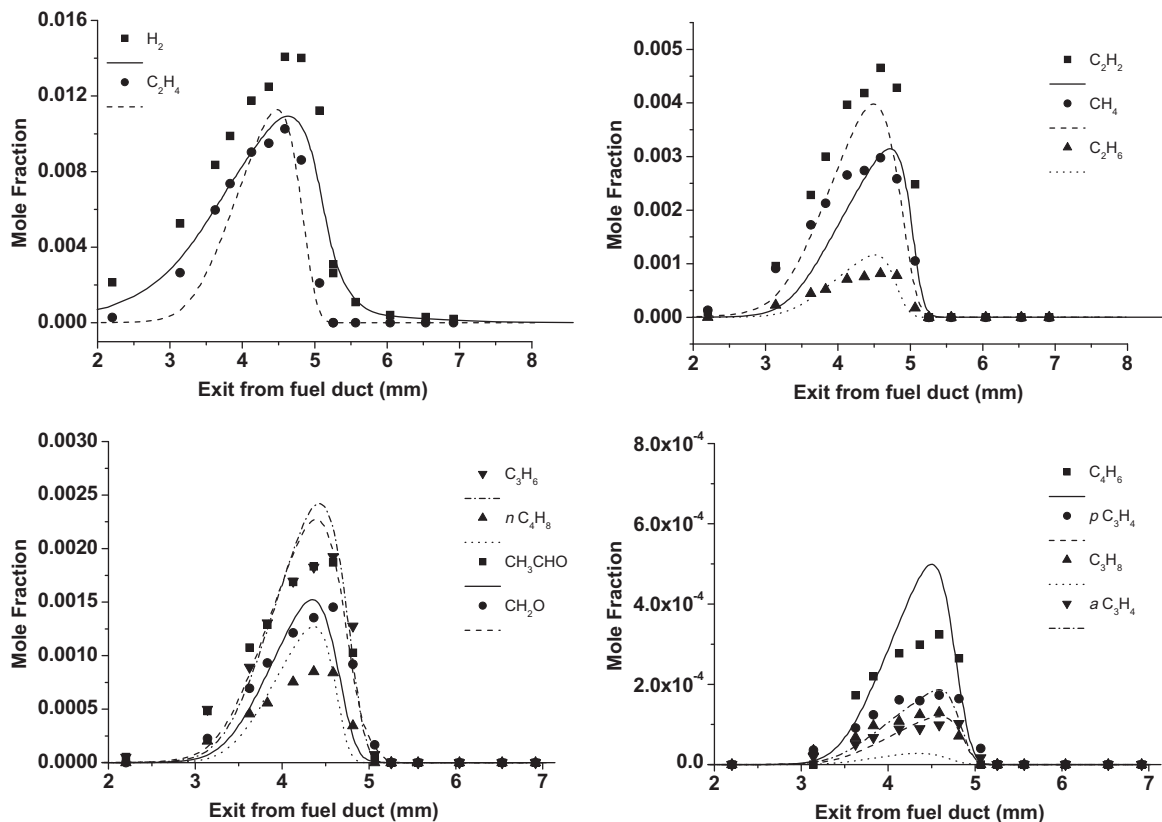


Fig. 21. Profile mole fraction of various species as a function of distance from the fuel boundary for non-premixed n-butanol flame at a value of the strain rate $a_2 = 100 \text{ s}^{-1}$, and the stoichiometric mixture fraction $Z_{\text{st}} = 0.23$.

iso-C₄H₇ ⇌ CH₃ + C₃H₄, with a rate constant of $k = 1.0 \times 10^{13} \exp[-57,000/(RT)]$ [s⁻¹]. The addition of H to iso-C₄H₈ forms iso-butyl radical (iso-C₄H₉) and tert-butyl radical (tert-C₄H₉). The demethylation of iso-C₄H₉ radicals forms propene (C₃H₆), a precursor of the stable allyl radical (C₃H₅). Fig. 18 shows this chemical evolution. Recombination of OH and allyl radicals explains the formation of propenol (C₃H₅OH). The main decomposition products of propenol are acrolein (C₃H₄O) and H radicals. These species make a significant contribution to the ignition of the system. The sharp peak of H radicals corresponds to the maximum of CO concentration and the ignition of the system with CO₂ formation. These kinetic considerations clarify that the large deviations observed at high temperatures in Figs. 13–16 could primarily attributed to the successive reactions of allyl and methyl-allyl radicals more than to the primary reactions of butanols. Referring to the comparisons reported in Fig. 10, it is evident the relevant role of the molecular dehydration reaction with formation of iso-C₄H₈ over

the radical path with acetone formation in tert-butanol oxidation at 1050 K. Fig. 19 compares the relative importance of the different reactions paths when n-butanol or tert-butanol are oxidized in air at 1 bar and at stoichiometric conditions. These values are evaluated at 50% of fuel conversion. At 1600 K, this figure indicates that for n-butanol the relative importance of chain propagations reactions, molecular reactions and initiation reactions is ~50%, 20% and 30%, respectively.

At low temperatures, in the range 900–1000 K, radical chain propagation reactions prevail. The importance of the four centre molecular reactions appears in a different way for the two isomers tert-butanol and n-butanol. As already observed, molecular dehydration reaction largely dominates the tert-butanol decomposition in the temperature range 1000–1600 K, while it accounts only for 15–20% of n-butanol decomposition. Unimolecular decomposition reactions prevail for both of these isomers of butanol at high temperatures, due to the very high activation energies of these radical

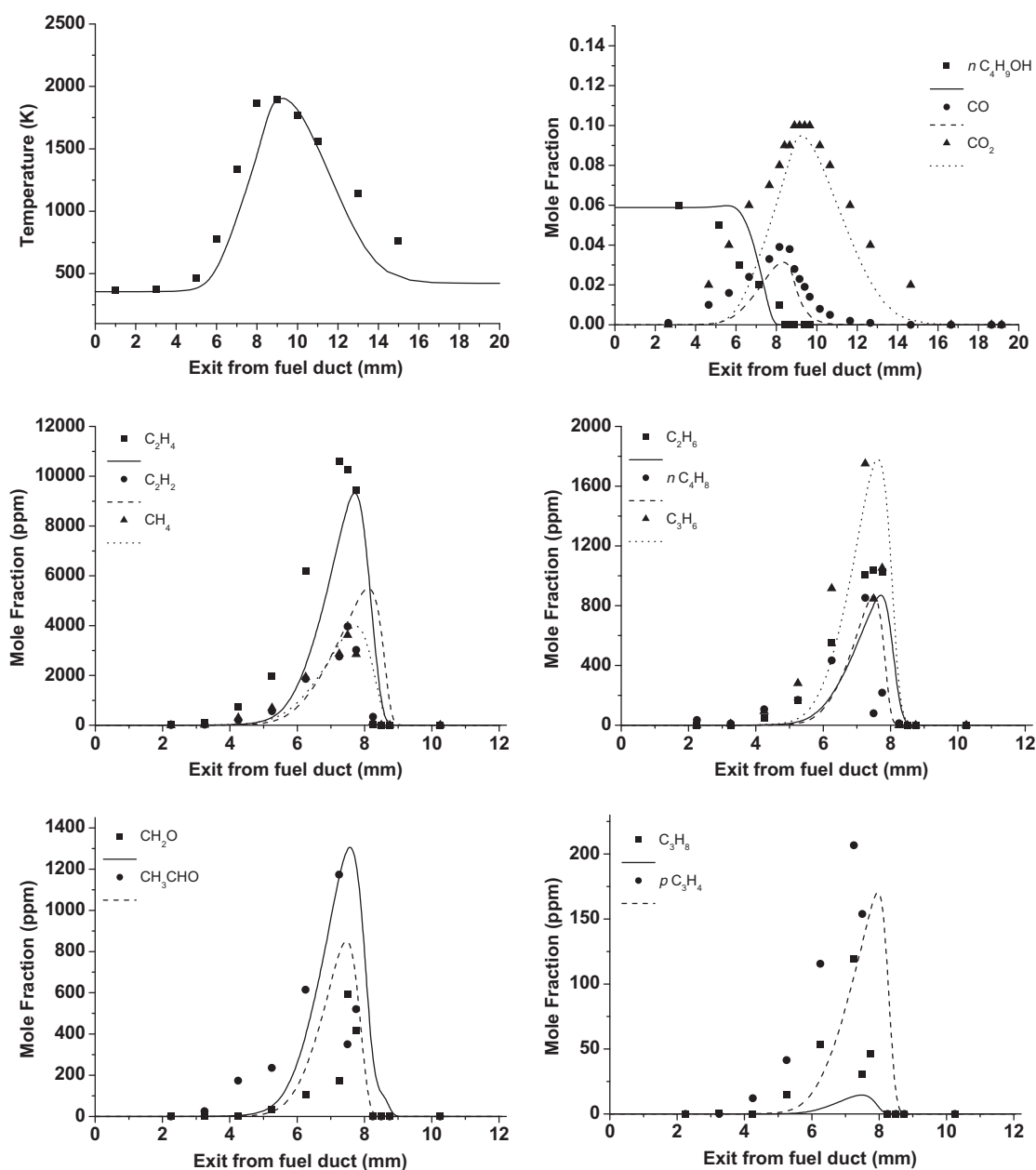


Fig. 22. Profiles of temperature and mole fraction of various species as a function of distance from the fuel boundary for non-premixed n-butanol flame [21] at a value of the strain rate $a_2 = 20 \text{ s}^{-1}$, and the stoichiometric mixture fraction $Z_{st} = 0.5283$.

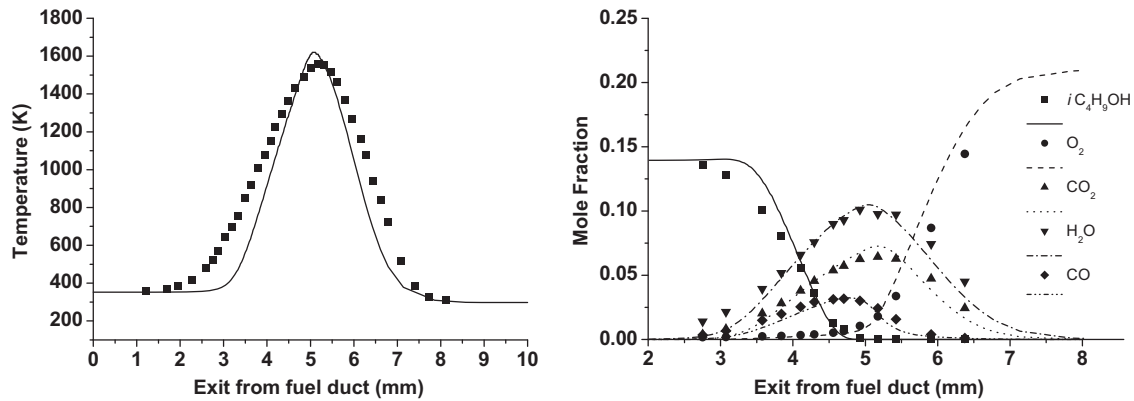


Fig. 23. Profile of temperature, and profiles of mole fraction of reactants, final products, and carbon monoxide as a function of distance from the fuel boundary for non-premixed iso-butanol flame. The strain rate $a_2 = 100 \text{ s}^{-1}$, and the stoichiometric mixture fraction $Z_{st} = 0.23$. The figure shows temperature profiles, measured using the coated thermocouple, and corrected to account for radiative heat losses from the wire.

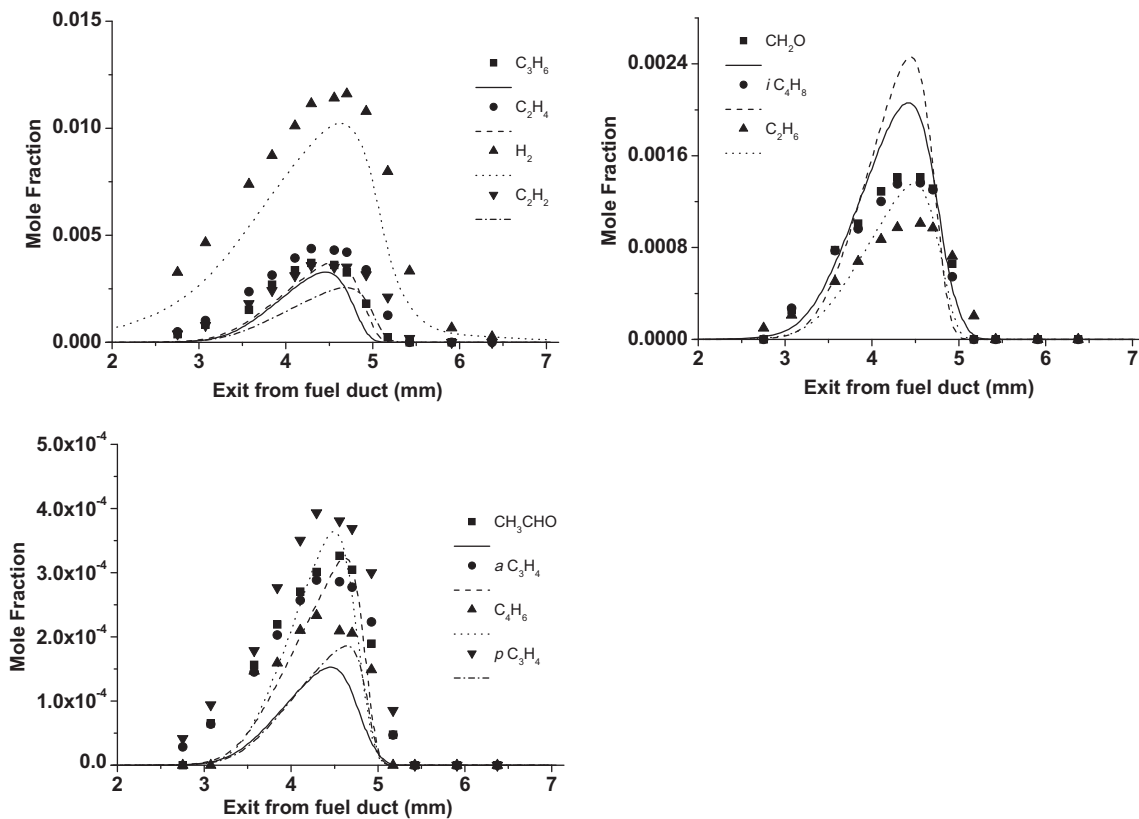


Fig. 24. Profile mole fraction of various species as a function of distance from the fuel boundary for non-premixed iso-butanol flame at a value of the strain rate $a_2 = 100 \text{ s}^{-1}$, and the stoichiometric mixture fraction $Z_{st} = 0.23$.

initiation reactions. Similarly, molecular dehydration of iso-butanol accounts for 20%, while the reactions to form both 1- C_4H_8 and 2- C_4H_8 from sec-butanol account for 40%.

5.5. Non-premixed flame of n-butanol and iso-butanol

Experimental measurements of the structure of counterflow non-premixed flame of n-butanol, discussed in Section 2, are compared with model predictions in Figs. 20 and 21. Fig. 20 shows the temperature profile measured using the bare (uncoated) thermocouple and the coated thermocouple. The measured values of the temperature are the same everywhere except in the vicinity of the position of maximum temperature. The maximum temperature

recorded by the uncoated thermocouple is about 200 K higher than that measured using the coated thermocouple. This indicates that the chemical reactions are not in equilibrium near the location where the temperature is the highest. As a consequence, there is catalytic heating on the surface of the uncoated thermocouple. The predicted temperature profile is slightly narrow when compared with experimental data obtained using the coated thermocouple. The agreement is considered to be satisfactory. Figs. 20 and 21 compare the predicted profiles of various species with experimental data. The predicted profiles of the reactants n- C_4H_9OH , and O_2 , final products CO_2 and H_2O , and the key intermediates H_2 and CO agree well with experimental data. The predicted and measured profiles show that the peak values of CO and H_2 are

located at the position where the concentration of fuel is very small. The peak values of CO_2 , H_2O and temperature are observed on the right side of the position where the concentration of fuel is very small. This is consistent with the asymptotic description of flame structure where the reaction zone is separated into two layers—an inner layer and an outer layer [3–5]. In the inner-layer, butanol reacts with radicals and the final intermediates formed are CO and H_2 . These intermediates are oxidized to CO_2 and H_2O in the outer-layer. The predicted profiles of CH_4 , C_2H_2 , C_2H_4 , C_2H_6 , C_3H_6 , C_4H_6 and C_4H_8 agree well with the measurements. Butanol was also detected in the n-butanol flame. The measured concentrations were very low. Therefore, they are not shown in Fig. 21.

Fig. 22 compares predictions of structure of n-butanol flame with experimental data of Sarathy et al. [21]. Comparison of the Figs. 20 and 21 with Fig. 22 highlights the influence of strain rate and stoichiometric mixture fraction on flame structure. These data are useful both in order to confirm the experimental measurements and to verify the possible systematic deviations between model predictions and experiments. There are a number of similarities between the two flames. The overall agreement between the predicted and measured profiles of intermediate species is satisfactory. Figs. 21 and 22 show that the predicted mole fraction of formaldehyde (CH_2O) is higher than the measurements. The predicted mole fraction of acetaldehyde (CH_3CHO) in Fig. 21 is less than the measurements. These deviations are not observed in the n-butanol oxidation in the JSR experiments reported in Figs. 11 and 12. Although, predictions of butadiene (C_4H_6) agrees reasonably well with the measurements in Fig. 22, they are higher than the measurements shown in Fig. 21. The same deviations were also

observed between predictions and measurements in Sarathy et al. [21].

Figs. 23 and 24 compare predictions of the kinetic model of the structure of non-premixed iso-butanol flame with experimental data. The iso-butanol flame structure was measured at conditions identical to those shown in Figs. 20 and 21 for n-butanol. The maximum value of the temperature recorded by the uncoated thermocouple is about 200 K higher than that measured using the coated thermocouple. The predicted temperature profile agrees well with the measurements obtained using the coated thermocouple. The predicted profiles of the n- $\text{C}_4\text{H}_9\text{OH}$, O_2 , CO_2 , H_2O , CO , H_2 , C_2H_4 , C_2H_2 and C_3H_6 agree well with the measurements. The asymptotic flame structure constructed from the profiles of the reactants, products and major intermediates is similar to that of n-butanol. Temperature profiles of the n-butanol and iso-butanol flames shown in Figs. 20 and 23 are similar, due to the same boundary conditions employed. Comparison of Figs. 21 and 24 show that the mole fractions of CH_2O are similar, while the mole fraction of CH_3CHO is lower in the iso-butanol flame. Trace amounts of butanol was observed in the n-butanol flame but none in the iso-butanol flame.

6. Summary and conclusions

A kinetic mechanism, that describes the primary reactions of pyrolysis and combustion of butanol isomers, is developed. This mechanism is appended to a previously developed detailed scheme of pyrolysis and oxidation of hydrocarbon fuels. Employing a systematic approach for the different reaction classes, including

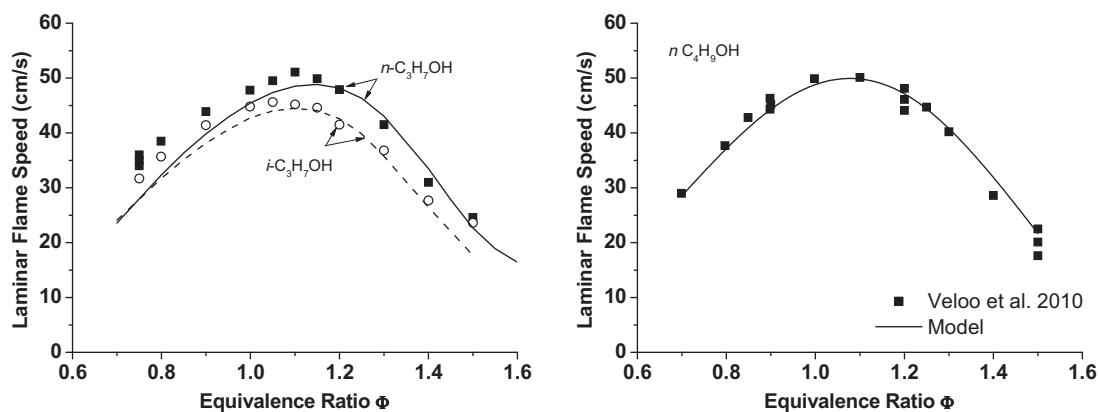


Fig. 25. The flame velocity of n-propanol, iso-propanol and n-butanol in air [63,64] as a function of equivalence ratio ($P = 1$ atm and $T_0 = 343$ K).

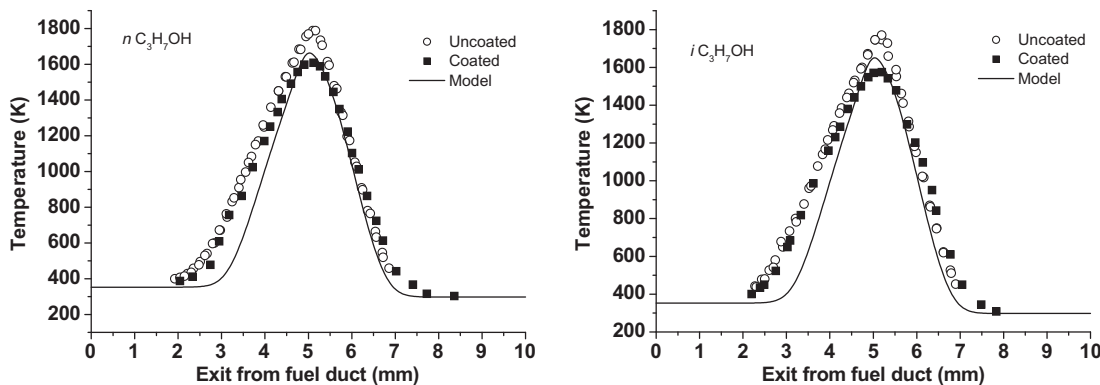


Fig. 26. Profile of temperature as a function of distance from the fuel boundary for non-premixed n-propanol flame and non-premixed iso-propanol flame. The strain rate $a_2 = 97.5 \text{ s}^{-1}$, and the stoichiometric mixture fraction $Z_{st} = 0.2449$. The figure shows temperature profiles measured using bare thermocouple and coated thermocouple. The profiles corrected for radiative heat losses.

four-center molecular dehydration reactions to form butenes, a small subset of new primary reactions were proposed for describing combustion of butyl alcohols. This kinetic model does not include low temperature reactions. To our knowledge, the batch experiments of Cullis and Warwicker [61] with the four isomers of butanol at 550–700 K are the only low temperature experimental data. Further low temperature data refer to n-heptane/n-butanol mixtures in the Orleans JSR [62] where the prevailing role of peroxy radicals from n-heptane covers the n-butanol effect. The expected weak effect of low temperature mechanisms of butanol isomers requires further dedicated experimental investigation.

New experimental data on counterflow non-premixed flame of n-butanol and iso-butanol were obtained for mechanism validation. Flame structures were measured under the same conditions for both fuels to elucidate the similarities and differences in combustion characteristics of the two isomers. The measured species profiles include those of formaldehyde and acetaldehyde. The validation of the kinetic model was extended to different sets of experimental data obtained by other investigators in very different operative conditions and experimental configurations. The agreement between the kinetic model and experimental data was generally satisfactory, in terms of reactivity and selectivity in major products and minor species. The flame structures and overall combustion characteristics of the four butanol isomers are found to be similar and also similar to those of the two propanol isomers. Similarity of flame velocity in combustible mixtures containing n-propanol and n-butanol further confirms this. Fig. 25 shows that predictions of the flame velocity of the kinetic model agree well with experimental data in Ref. [63] and Ref. [64]. The kinetic model developed here, together with the reference kinetic parameters of reactions involving the presence of hydroxyl group, is a useful starting point for extension to higher alcohols.

Acknowledgments

The Authors acknowledge the valuable discussions with Professor M. Dente and the useful work of A. Cuoci. The Authors further acknowledge Professors F.N. Egolfopoulos, Dr. C.K. Westbrook and Dr. P.S. Veloo for providing the experimental data on flame velocity of Fig. 25 prior to their publication. The research at Politecnico di Milano is supported by CNR-MAP (biofuel project) and by the European Union Seventh Framework Programme (FP7/2007–2013) under the DREAM Project Grant Agreement No. 211861. The research at the University of California at San Diego is supported by UC Discovery/Westbiofuels, Grant # GCP06-10228.

Appendix A. Temperature profiles of n-propanol and iso-propanol flames

An experimental and kinetic modeling study was carried out previously on n-propanol and iso-propanol combustion [15]. In this study the structures of counterflow flames of n-propanol and iso-propanol were measured using the burner and procedures described here. The measurements were made for $Y_{F,1} = 0.3$, $T_1 = 353$ K, $Y_{O_2,2} = 0.233$, $T_2 = 298$ K, $a_2 = 97.5$ s⁻¹, $V_1 = 0.235$ m/s, $V_2 = 0.25$ m/s, and $L = 10$ mm. At these conditions the stoichiometric mixture fraction $Z_{st} = 0.2449$. In this previous study the measured temperature profile was not shown, because it was not available. The temperature profiles were measured using the bare and coated thermocouple and are shown in Fig. 26. The procedure is the same as described here. The temperature measured by the bare thermocouple is higher than that recorded by the coated thermocouple. This clearly indicates that there is catalytic heating of the bare wire. Fig. 26 shows that the predictions of the kinetic model agree with the experimental data.

References

- [1] T.S. Norton, F.L. Dryer, Proc. Combust. Inst. 23 (1990) 179–185.
- [2] T.J. Held, F.L. Dryer, Proc. Combust. Inst. 25 (1994) 901–908.
- [3] B. Yang, K. Seshadri, Combust. Sci. Technol. 97 (1994) 193–218.
- [4] K. Seshadri, F.A. Williams, Reduced chemical systems and their application in turbulent combustion, in: P.A. Libby, F.A. Williams (Eds.), Turbulent Reacting Flows, Academic Press, San Diego, CA, 1994, pp. 153–210.
- [5] K. Seshadri, Proc. Combust. Inst. 26 (1996) 831–846.
- [6] S.C. Li, F.A. Williams, Proc. Combust. Inst. 26 (1996) 1017–1024.
- [7] F.N. Egolfopoulos, D.X. Lu, C.K. Law, Proc. Combust. Inst. 24 (1992) 833–841.
- [8] N. Marinov, Int. J. Chem. Kinet. 31 (1999) 183–220.
- [9] W. Tsang, Int. J. Chem. Kinet. 36 (8) (2004) 456–465.
- [10] P. Saxena, F.A. Williams, Proc. Combust. Inst. 31 (2007) 1149–1156.
- [11] R. Seiser, S. Humer, K. Seshadri, E. Pucher, Proc. Combust. Inst. 31 (2007) 1173–1180.
- [12] P. Dagaut, C. Togbé, Energy Fuels 22 (2008) 3499–3505.
- [13] M. Abián, C. Esarte, A.A. Millera, R. Bilbao, M.U. Alzueta, Energy Fuels 22 (2008) 3814–3823.
- [14] A. Frassoldati, A. Cuoci, T. Faravelli, E. Ranzi, Combust. Sci. Technol., in press.
- [15] A. Frassoldati, A. Cuoci, T. Faravelli, U. Niemann, E. Ranzi, R. Seiser, K. Seshadri, Combust. Flame 157 (2010) 2–16.
- [16] P. Dagaut, C. Togbé, Fuel 87 (2008) 3313–3321.
- [17] J. Moss, A.M. Berkowitz, M.A. Oehlschlaeger, J. Biet, A. Warth, P.A. Glaude, F. Battin-Leclerc, J. Phys. Chem. 112 (2008) 10843–10855.
- [18] G. Black, H. Curran, S. Pichon, J. Simmie, V. Zhukov, Combust. Flame 157 (2010) 363–373.
- [19] C. McEnally, L.D. Pfefferle, Proc. Combust. Inst. 30 (2005) 1363–1370.
- [20] B. Yang, P. Oßwald, Y. Li, J. Wang, L. Wei, Z. Tian, F. Qi, K. Kohe-Höinghaus, Combust. Flame 148 (2007) 198–209.
- [21] S.M. Sarathy, M.J. Thomson, C. Togbé, P. Dagaut, F. Halter, C. Mountaim-Rousselle, Combust. Flame 156 (2008) 852–864.
- [22] F.A. Williams, Combustion Theory, second ed., Addison-Wesley Publishing Company, Redwood City, CA, 1985.
- [23] A. Liñán, F.A. Williams, Fundamental aspects of combustion, Oxford Engineering Science Series, vol. 34, Oxford University Press, New York, 1993.
- [24] N. Peters, Combust. Sci. Technol. 30 (1983) 1–17.
- [25] N. Peters, Turbulent Combustion, Cambridge University Press, Cambridge, England, 2000.
- [26] K. Seshadri, F.A. Williams, Int. J. Heat Mass Transfer 21 (2) (1978) 251–253.
- [27] J.H. Kent, Combust. Flame 14 (1970) 279–282.
- [28] R.C. Peterson, N.M. Laurendeau, Combust. Flame 60 (1985) 279–284.
- [29] E. Ranzi, M. Dente, T. Faravelli, G. Pennati, Combust. Sci. Technol. 95 (1994) 1–50.
- [30] A. Galano, J.R. Alvarez-Idaboy, G. Bravo-Perez, M.E. Ruiz-Santoyo, Phys. Chem. Chem. Phys. 4 (2002) 4648–4662.
- [31] R. Atkinson, D.L. Baulch, R.A. Cox, R.F.H.J.A. Kerr Jr., M.J. Rossi, J. Troe, J. Phys. Chem. Ref. Data 26 (1997) 521–1011.
- [32] R. Atkinson, D.L. Baulch, R.A. Cox, R.F.H.J.A. Kerr Jr., M.J. Rossi, J. Troe, J. Phys. Chem. Ref. Data 28 (1999) 191–394.
- [33] E. Ranzi, A. Sogaro, P. Gaffuri, G. Pennati, C.K. Westbrook, W.J. Pitz, Combust. Flame 99 (1994) 201–211.
- [34] H.J. Curran, Int. J. Chem. Kinet. 38 (4) (2006) 250–275.
- [35] S.W. Benson, Thermochemical Kinetics, second ed., Wiley, New York, 1996.
- [36] H.J. Curran, P. Gaffuri, W.J. Pitz, C.K. Westbrook, A comprehensive modeling study of n-heptane oxidation, Combust. Flame 114 (1998) 149–177.
- [37] M. Dente, G. Bozzano, T. Faravelli, A. Marongiu, S. Pierucci, E. Ranzi, Modeling of pyrolysis processes in gas and condensed phase, in: G. Marin (Ed.), Advances in Chemical Engineering, vol. 32, 2007, pp. 52–166.
- [38] J. Moc, J.M. Simmie, H.J. Curran, J. Mol. Struct. 928 (2009) 149–157.
- [39] C.G. Newman, H.E. O'Neal, M.A. Ring, F. Leska, N. Shipley, Int. J. Chem. Kinet. 11 (1979) 1167–1182.
- [40] B.H. Bui, R.S. Zhu, M.C. Lin, J. Chem. Phys. 117 (24) (2002) 11188.
- [41] M. Dente, Personal Communication, 2009.
- [42] E. Ranzi, A. Sogaro, P. Gaffuri, G. Pennati, T. Faravelli, Combust. Sci. Technol. 96 (1994) 279–325.
- [43] E. Ranzi, M. Dente, A. Goldaniga, G. Bozzano, T. Faravelli, Prog. Energy Combust. Sci. 27 (2001) 99–139.
- [44] E. Ranzi, T. Faravelli, A. Frassoldati, S. Granata, Ind. Eng. Chem. 44 (2005) 5170–5183.
- [45] E. Ranzi, Energy Fuels 20 (2006) 1024–1032.
- [46] R.J. Kee, F. Rupley, J.A. Miller, The Chemkin Thermodynamic Data Base, Report SAND86-8215B, Sandia National Laboratories, Livermore, CA, 1987.
- [47] R.J. Kee, F. Rupley, J.A. Miller, The Chemkin Thermodynamic Data Base, Technical Report, Sandia National Laboratories, Livermore, CA, 1989.
- [48] <http://www.chem.polimi.it/CRECKModeling>.
- [49] D. Manca, G. Buzzi-Ferraris, T. Faravelli, E. Ranzi, Combust. Theory Modell. 5 (2) (2001) 185–199.
- [50] A. Cuoci, A. Frassoldati, T. Faravelli, E. Ranzi, Frequency response of counter flow diffusion flames to strain rate harmonic oscillations, Combust. Sci. Technol. 180 (2008) 767–784.
- [51] G. Buzzi-Ferraris, Building Numerical Libraries the Object-Oriented Way, Addison Wesley/Longman, 1993.
- [52] G. Buzzi-Ferraris, Numerical Libraries in C++, Politecnico di Milano. <<http://www.chem.polimi.it/homes/gbuzzi>>.

- [53] R. Schultz, G.B. Kistiakowsky, *J. Am. Chem. Soc.* 56 (1934) 395–398.
- [54] J.A. Barnard, *Trans. Faraday Soc.* 53 (1957) 1423–1430.
- [55] J.A. Barnard, The pyrolysis of tert-butanol, *Trans. Faraday Soc.* 54 (1958) 947–951.
- [56] T.K. Choudhury, M.C.L.M.C.C.-Y. Lin, W.A. Sanders, *Combust. Sci. Technol.* 71 (1990) 219–232.
- [57] P. Dagaut, S.M. Sarathy, M.J. Thomson, *Proc. Combust. Inst.* 32 (2009) 229–234.
- [58] Z. Zhao, M. Chaos, A. Kazakov, F.L. Dryer, *Int. J. Chem. Kinet.* 40 (2008) 1–18.
- [59] S. Pichon, G. Black, N. Chaumeix, M. Yahyaoui, J.M. Simmie, H.J. Curran, R. Donohue, *Combust. Flame* 156 (2009) 494–504.
- [60] S. Saxena, J.H. Kiefer, S.J. Klippenstein, *Proc. Combust. Inst.* 32 (2009) 123–130.
- [61] C.F. Cullis, E.A. Warwicker, *Proc. Roy. Soc.* 264 (1318) (1961) 392–407.
- [62] P. Dagaut, C. Togbé, *Energy Fuels* 23 (7) (2009) 3527–3535.
- [63] P. Veloo, F. Egolfopoulos, C. Westbrook, Studies of n-propanol/air and isopropanol/air premixed flames. 2009 Fall Meeting of the Western States Section of the Combustion Institute, 2009.
- [64] P.S. Veloo, Y.L. Wang, F.N. Egolfopoulos, C.K. Westbrook, *Combust. Flame* 157 (2010) 1989–2004.